NAVAL POSTGRADUATE SCHOOL

MONTEREY, CALIFORNIA

THESIS

THERMODYNAMIC SYSTEM ANALYSIS OF A LIQUID AIR ENERGY STORAGE SYSTEM

by

Todd A. Howe

June 2018

Thesis Advisor: Anthony G. Pollman
Second Reader: Eugene P. Paulo

Approved for public release. Distribution is unlimited.

THIS PAGE INTENTIONALLY LEFT BLANK

REPORT DOCUMENTATION PAGE	Form Approved OMB No. 0704-0188

Public reporting burden for this collection of information is estimated to average 1 hour per response, including the time for reviewing instruction, searching existing data sources, gathering and maintaining the data needed, and completing and reviewing the collection of information. Send comments regarding this burden estimate or any other aspect of this collection of information, including suggestions for reducing this burden, to Washington headquarters Services, Directorate for Information Operations and Reports, 1215 Jefferson Davis Highway, Suite 1204, Arlington, VA 22202-4302, and to the Office of Management and Budget, Paperwork Reduction Project (0704-0188) Washington, DC 20503.

1. AGENCY USE ONLY *(Leave blank)*	2. REPORT DATE June 2018	3. REPORT TYPE AND DATES COVERED Master's thesis

4. TITLE AND SUBTITLE
THERMODYNAMIC SYSTEM ANALYSIS OF A LIQUID AIR ENERGY STORAGE SYSTEM

5. FUNDING NUMBERS

6. AUTHOR(S) Todd A. Howe

7. PERFORMING ORGANIZATION NAME(S) AND ADDRESS(ES)
Naval Postgraduate School
Monterey, CA 93943-5000

8. PERFORMING ORGANIZATION REPORT NUMBER

9. SPONSORING / MONITORING AGENCY NAME(S) AND ADDRESS(ES)
N/A

10. SPONSORING / MONITORING AGENCY REPORT NUMBER

11. SUPPLEMENTARY NOTES The views expressed in this thesis are those of the author and do not reflect the official policy or position of the Department of Defense or the U.S. Government.

12a. DISTRIBUTION / AVAILABILITY STATEMENT
Approved for public release. Distribution is unlimited.

12b. DISTRIBUTION CODE
A

13. ABSTRACT (maximum 200 words)

Renewable energy generation is intermittent, necessitating energy storage subsystems to provide electricity during periods of reduced or no power generation. Liquid air energy storage (LAES) systems, with their high energy density and scalability, are a promising method to store energy for intermittent systems. This thesis presents two independent papers for use in the systems engineering process during the conceptualization and requirements stage of designing and development a LAES system. The first paper is a closed-form method of calculating the compressor work for a modified simple Linde-Hampson system and liquid yield of a binary mixture of nitrogen and oxygen using only their respective pure fluid tables. This tool provides a methodology to check holistically a vast amount of different potential binary mixtures for use in a LAES system. The second paper is an energy and exergy analysis of a LAES system in order to map the trade space and identify optimum operating ranges. Additionally, this paper provides insight in to potential measures of performance and effectiveness of the LAES system. Finally, this thesis presents a valuable Excel add-in tool used to download fluid chemistry tables from the National Institute of Standards and Technology website.

14. SUBJECT TERMS
liquid air energy storage, energy storage, cyrogenic system, binary mixture, liquefaction system, thermodynamic analysis, energy analysis, exergy analysis, systems engineering tool, NIST Caddie

15. NUMBER OF PAGES 97

16. PRICE CODE

17. SECURITY CLASSIFICATION OF REPORT	18. SECURITY CLASSIFICATION OF THIS PAGE	19. SECURITY CLASSIFICATION OF ABSTRACT	20. LIMITATION OF ABSTRACT
Unclassified	Unclassified	Unclassified	UU

NSN 7540-01-280-5500

Standard Form 298 (Rev. 2-89)
Prescribed by ANSI Std. 239-18

THIS PAGE INTENTIONALLY LEFT BLANK

Approved for public release. Distribution is unlimited.

THERMODYNAMIC SYSTEM ANALYSIS OF A LIQUID AIR ENERGY STORAGE SYSTEM

Todd A. Howe
Captain, United States Army
BSME, Norwich University, 2008

Submitted in partial fulfillment of the
requirements for the degree of

MASTER OF SCIENCE IN SYSTEMS ENGINEERING

from the

NAVAL POSTGRADUATE SCHOOL
June 2018

Approved by: Anthony G. Pollman
Advisor

Eugene P. Paulo
Second Reader

Ronald E. Giachetti
Chair, Department of Systems Engineering

THIS PAGE INTENTIONALLY LEFT BLANK

ABSTRACT

Renewable energy generation is intermittent, necessitating energy storage subsystems to provide electricity during periods of reduced or no power generation. Liquid air energy storage (LAES) systems, with their high energy density and scalability, are a promising method to store energy for intermittent systems. This thesis presents two independent papers for use in the systems engineering process during the conceptualization and requirements stage of designing and development a LAES system. The first paper is a closed-form method of calculating the compressor work for a modified simple Linde-Hampson system and liquid yield of a binary mixture of nitrogen and oxygen using only their respective pure fluid tables. This tool provides a methodology to check holistically a vast amount of different potential binary mixtures for use in a LAES system. The second paper is an energy and exergy analysis of a LAES system in order to map the trade space and identify optimum operating ranges. Additionally, this paper provides insight in to potential measures of performance and effectiveness of the LAES system. Finally, this thesis presents a valuable Excel add-in tool used to download fluid chemistry tables from the National Institute of Standards and Technology website.

THIS PAGE INTENTIONALLY LEFT BLANK

TABLE OF CONTENTS

I. INTRODUCTION 1
- A. MOTIVATION AND BACKGROUND 1
- B. LIQUID AIR ENERGY STORAGE 2
- C. THESIS OVERVIEW 3

II. CURRENT LIQUID AIR ENERGY STORAGE SYSTEM OF INTEREST 7
- A. SYSTEM DESCRIPTION 7
- B. SYSTEM DYNAMICS 10

III. PAPER I: CLOSED-FORM THERMODYNAMIC ANALYSIS OF A MODIFIED LINDE-HAMPSON SYSTEM WITH BINARY MIXTURES 13
- A. ABSTRACT 13
- B. INTRODUCTION 13
- C. SIMPLE LINDE-HAMPSON SYSTEM ANALYSIS 15
- D. MODIFIED LH SYSTEM WITH A BINARY MIXTURE 20
- E. RESULTS AND DISCUSSION 24
- F. CONCLUSIONS 27
- G. ACKNOWLEDGMENTS 28

IV. PAPER II: OPERATING RANGE FOR AN IDEAL BUILDING-SCALE LAES SYSTEM THROUGH ENERGY AND EXERGY ANALYSIS 29
- A. ABSTRACT 29
- B. INTRODUCTION 29
- C. SYSTEM DESCRIPTION 31
- D. SYSTEM ENERGY ANALYSIS 33
  - 1. Liquefaction Subsystem 34
  - 2. Energy Production Subsystem 35
  - 3. Complete LAES System 36
- E. SYSTEM EXERGY ANALYSIS 37
  - 1. Liquefaction Subsystem 38
  - 2. Energy Production Subsystem 40
  - 3. Complete LAES System 41
- F. RESULTS AND DISCUSSION 41
  - 1. First Law Results and Discussion 41

2. Second Law Results and Discussion 49
G. CONCLUSION 53
H. ACKNOWLEDGMENTS 54

V. NIST CADDIE 55
A. BACKGROUND AND INTRODUCTION 55
B. NIST CADDIE SETUP AND INSTRUCTIONS 57

VI. CONCLUSION AND FUTURE WORK 61

APPENDIX A. NOMENCLATURE FOR CHAPTER III AND IV 65
1. CHAPTER III NOMENCLATURE 65
2. CHAPTER IV NOMENCLATURE 65

APPENDIX B. SUPPLEMENTAL NIST CADDIE EXCEL ADD-IN 67

LIST OF REFERENCES 69

INITIAL DISTRIBUTION LIST 73

LIST OF FIGURES

Figure 1. System Level Diagram of a LAES System. 3

Figure 2. V-Model Example Showing Where Current Thesis is Targeted. Adapted from Blanchard and Fabrycky (2010) and Forsberg and Mooz (1992) 4

Figure 3. Schematic of the Nitro-Turbodyne, Inc. LAES System. Adapted from Nitro-Turbodyne (2016). 7

Figure 4. Image of the Molecular Sieve as Part of the Nitro-Turbodyne, Inc. LAES System. Adapted from Nitro-Turbodyne (2016). 8

Figure 5. Image of the Compressor as Part of the Nitro-Turbodyne, Inc. LAES System. Source: Nitro-Turbodyne (2016) 9

Figure 6. Image of the Ice-Bath Heat Exchanger as Part of the Nitro-Turbodyne, Inc. LAES System. Source: Nitro-Turbodyne (2016). 9

Figure 7. Image of the Condenser Subsystem as Part of the Nitro-Turbodyne, Inc. LAES System. Adapted from Nitro-Turbodyne (2016). 9

Figure 8. Block Diagram of Nitro-Turbodyne, Inc. LAES System 11

Figure 9. Simple Linde-Hampson Liquefaction System. Adapted from Barron (1985). 14

Figure 10. Diagram of Simple Linde-Hampson Cycle. Adapted from Barron (1985). 15

Figure 11. VLE Diagram of an Oxygen and Nitrogen Mixture 19

Figure 12. Modified Linde-Hampson System with Two Compressors 20

Figure 13. Composition of Nitrogen and Oxygen versus Work per Unit Mass Compressed (kJ/kg). 26

Figure 14. Composition of Nitrogen and Oxygen versus Figure of Merit. 27

Figure 15. System Diagram of a Liquid Air Energy Storage System. 31

Figure 16. Air Temperature Entropy Diagram Showing Each State in the LAES System. 33

Figure 17. Liquid Yield for Simple Linde-Hampson Subsystem over Varying State 2 Pressures. 42

Figure 18. Air Temperature Entropy Diagram Showing Liquid Yield with Lines of Constant Enthalpy from State 3 to State 4.....43

Figure 19. Compressor Work per Unit Mass Liquefied for Simple Linde-Hampson Subsystem. 44

Figure 20. Liquid Yield for Pre-cooled Linde-Hampson Subsystem with Varying State 2 Pressures. 44

Figure 21. Compressor Work for Pre-cooled Linde Subsystem with Varying State 2 Pressures. 45

Figure 22. Required Heat Removal for Pre-cooled Linde-Hampson Subsystem.....46

Figure 23. Total Work per Unit Mass Liquefied for the Pre-cooled Liquefaction Subsystem. 46

Figure 24. Resulting LAES System Energy Efficiency with Varying State 2 and 7 Pressures and Three State 2' Temperatures. 47

Figure 25. Resulting LAES System Energy Efficiency over Full Range State 7 Pressures and three Selected State 2' Temperatures and State 2 Pressures. 48

Figure 26. Effects of Increasing State 8 Temperature on LAES Energy Efficiency at a State 2' Temperature of 250K and State 7 Pressure of 100 MPa. 49

Figure 27. JT Valve Exergetic Efficiency with Varying State 2 Pressures and State 2' Temperatures. 50

Figure 28. HX-1 Exergetic Efficiency with Varying State 2 Pressures and State 2' Temperatures. 51

Figure 29. Exergy Destruction Comparison of the JT Valve and HX-1 at a State 2 Pressure of 20 MPa over varying State 2' Temperatures. 51

Figure 30. Exergetic Efficiency of the Liquefaction Subsystem.....52

Figure 31. LAES System Exergetic Efficiency at a State 7 Pressure of 100 MPa and State 8 Temperature of 300 K. 53

Figure 32. NIST Caddie Flowchart. 56

Figure 33. Image of the Primary Excel User Form in the NIST Caddie. 58

Figure 34. NIST Caddie Isothermal Data Type User Form. 59

Figure 35. Nomenclature for Chapter III.....65

Figure 36. Nomenclature for Chapter IV. 65

Figure 37. Six Main Excel User Forms with User Input Options in NIST Caddie.....67

THIS PAGE INTENTIONALLY LEFT BLANK

LIST OF TABLES

Table 1. Performance of the Linde-Hampson Cycle.....17

Table 2. Molar Fractions and Partial Pressures for Nitrogen and Oxygen and Different States. 25

Table 3. Results for Nitrogen and Oxygen Mixture in Modified Linde Hampson System. 25

Table 4. List of Iso-Pressures Available from Lemmon et al. 41

THIS PAGE INTENTIONALLY LEFT BLANK

LIST OF ACRONYMS AND ABBREVIATIONS

atm	atmospheres
CAES	compressed air energy storage
C4I	command, control, communications, computers, and intelligence
COTS	commercial-off-the-shelf
ESTEP	Energy Systems Technology Evaluation Program
FOB	forward operating base
FOM	figure of merit
HX	heat exchanger
JT	Joule Thomson
LAES	liquid air energy storage
LH	Linde-Hampson
MPa	mega Pascal
NAVFAC	Naval Facilities Engineering Command
NIST	National Institute of Standards and Technology
NPS	Naval Postgraduate School
ONR	Office of Naval Research
PHS	pumped-hydroelectric storage
VBA	Visual Basic for Applications
VLE	vapor-liquid equilibrium

THIS PAGE INTENTIONALLY LEFT BLANK

EXECUTIVE SUMMARY

A key objective of the Marine Corps Expeditionary Energy Strategy Planning Guidance developed in 2011 was to "allow Marines to travel lighter – with less – and move faster by reducing size and amount of equipment and dependence on bulk supplies" (USMC 2011). The planning guidance states, "energy is an essential combat enabler and a critical vulnerability" (USMC 2011). One of these vulnerabilities lies in the dependence on fossil fuels to provide needed energy to operate command posts in expeditionary environments. According to the planning guidance, this dependence has caused the Marine Corps to consume over 200,000 gallons of fuel per day at Afghanistan forward operating bases in 2010 (USMC 2011). The Army's Energy Security and Sustainability Strategy states similar goals of decreasing the force's demand of fossil fuels and diversifying and expanding resource supplies (ASAIE 2015). Solar and wind technologies can potentially provide a portion of all of the necessary power reducing or eliminating use of fossil fuels. However, these generation sources are intermittent and are faced with periods of reduced or no power generation. A solution to this problem is energy storage technologies, and this thesis presents one technology known as liquid air energy storage (LAES).

Liquid air energy storage systems are capable of operating completely independent of fossil fuels. The system uses excess power from renewable energy sources such as solar and wind to power equipment necessary to produce liquid air. Liquid air energy storage systems condense air to a liquid at -196°C, store it in an insulated unpressurized vessel, and expand the liquid air through a turbine when electricity is in demand (Gökçeer, Demirkaya, and Padilla 2017). In order to design and develop such a system, systems engineers are in need of tools to support their understanding of the physics and thermodynamics of a LAES system, a method to analyze performance parameters, and a means of validating modeling and simulation to support model-based systems engineering.

This analysis thesis presents a methodology for a systems engineer to perform analysis and comparison of a vast array of cryogenic, non-reacting binary mixtures used in the liquefaction subsystem of the LAES system. The methodology provides a new, closed-form means to investigate alternative working fluids to air and mixtures used in an additional subsystem to pre-cool air, which results in higher liquid air yields. Additionally, this analysis thesis identifies optimum pressure ranges of 20 to 50 MPa exiting the air compressor. This operating range produces the highest liquid yields and results in the highest energy and exergetic efficiencies. The analysis identified pre-cooling of air in the liquefaction subsystem and heating of liquid air beyond ambient temperatures also resulted in higher liquid yields, and in energy and exergetic efficiencies. The work presented in this thesis provides the fundamental understanding of the physics and thermodynamics of a LAES system. Systems engineers conducting future modeling and simulation of a LAES system may reference the equations and methodology presented in this thesis to validate that their models are within the expected performance parameters and producing physically realistic output.

The thesis presents this body of knowledge in the form of two journal manuscripts. The two papers are titled "Closed-Form Thermodynamic Analysis of a Modified Linde-Hampson System with Binary Mixtures" and "Operating Range for an Ideal Building-Scale LAES System through Energy and Exergy Analysis" and are pending acceptance to *Energy* and *Entropy* journals, respectively. Additionally, the thesis presents the system description and system dynamics of the current LAES system in possession of the Naval Postgraduate School. Finally, the thesis presents an additional analytic tool, which downloads thermophysical fluid properties from the National Institute of Standards and Technology (NIST) website. The NIST chemistry webbook website limits users to view up to 600 rows of data in only html or a tab-delimited text file format. The tool, dubbed NIST Caddie, is capable of downloading up to 1,048,576 rows of data directly into an Excel worksheet. This enables a user to complete thermodynamic calculations completely in Excel over the entire range of fluid properties and render results seamlessly as Excel graphs and charts. This tool was vital to the analysis and methodology presented in the Chapter III of the thesis.

References

ASAIE, Department of the Army. 2015. Energy Security and Sustainability Strategy. RefID: 2-204FF1C. March 03. https://www.army.mil/e2/c/downloads/394128.pdf.

Gökçeer, Tonguç, Gökmen Demirkaya, and Ricardo Vasquez Padilla. 2017. "Thermoeconomic Analysis of Liquid Air Energy Storage System." *ASME 2017 11th International Conference on Energy Sustainability.* Charlotte, North Carolina: ASME Digital Collection. 1–9.

USMC. 2011. *USMC Expeditionary Energy Strategy Implementation Planning Guidance.* Arlington, VA: USMC Expeditionary Energy Office.

THIS PAGE INTENTIONALLY LEFT BLANK

ACKNOWLEDGMENTS

I would like to thank my advisor, co-author Dr. Pollman, and co-author Dr. Gannon for their amazing support and guidance throughout this process. Dr. Pollman, thank you for providing the vector adjustments throughout the thesis process, *no hand hold*. Dr. Gannon, thank you for the unparalleled expertise and keeping the door open for my somewhat frequent unannounced visits.

I would like to thank my amazing and supportive wife. Your strength and perseverance throughout these years has allowed me to maintain my focus through the long hours and late nights. We have had many changes over these two years, most of all, our wonderful son. Thank you so much for being such an incredible mother and wife: without your outstanding support, none of this would have been possible.

THIS PAGE INTENTIONALLY LEFT BLANK

I. INTRODUCTION

A. MOTIVATION AND BACKGROUND

Remote communities and military forward operating bases (FOBs) often do not have access to the traditional electrical grid. In these instances, they must rely on electrical generation methods like diesel or gas generators and/or renewable energy systems. When integrated, these systems form a microgrid. Microgrid systems are a localized energy grid designed to supply the necessary electrical load for a small community (Chowdhury, Chowdhury, and Crossley 2009). Microgrids normally act in two distinct modes, a stand-alone island mode and grid-connected mode (Chowdhury, Chowdhury, and Crossley 2009). A microgrid may consist of multiple types of distributed energy resources such as natural gas, biogas, wind power, solar photovoltaic cells, fuel cells, combined heat and power systems (Chowdhury, Chowdhury, and Crossley 2009). An added benefit to microgrids is there close proximity to demand, which "increases the power quality and reliability of electricity delivered to sensitive end-uses" (Hatziargyriou et al. 2007, 79).

Remote communities in developed countries and military operations have similar expectations of electrical service. Whether for quality of life, such as clothes washers and dryers, air-conditioners, electric ovens and ranges, or for mission-critical equipment, such as command, control, communications, computers, and intelligence (C4I) equipment, end-users have the expectation of sustained and reliable electrical services (Backhaus et al. 2015). In a situation where fuel resupply to either remote communities or military operations is delayed or unavailable, the choice is to rely on renewable energy systems within the microgrid or suffer outages.

In 2010, Marine Corps forward operating bases' total power generation was up to 303 MW and required over 200,000 gallons of fuel per day (Pollman 2003). Logistics burdens like these have made it a mission for the Marine Expeditionary Forces by 2025 to sustain its C4I and life support systems in place and only rely on liquid fuel for mobility systems (USMC 2011). The Army's Energy Security and Sustainability Strategy cites the use of microgrids and the need to decrease resource demand, drive innovation, and

diversify and expand resource supply (ASAIE 2015). In order to achieve a decreased demand of fossil fuels, the Marine Corps and Army must shift power generation away from diesel generators and more to renewable energy systems like solar and wind technologies.

Solar and wind renewable energy systems are considered intermittent energy systems, and they alone are not sufficient to provide sustained uninterrupted electrical loads. Intermittent energy systems on a remote microgrid must rely on energy storage if service is to remain uninterrupted. Renewable energy systems have periods of excess power and system shortages. When electrical generation is higher than the demand, energy storage systems uses the excess power to store energy and then release power during shortages in order to balance electrical loads (Wang et al. 2015).

B. LIQUID AIR ENERGY STORAGE

There are multiple options to balance electrical loads: rechargeable batteries, pumped hydro, compressed air, liquid air, and others. Given their high energy density and scalability, liquid air energy storage (LAES) systems are a promising method to store energy for intermittent systems (Wang et al. 2015). Batteries are a valid energy storage solution but can be costly overtime due to the need to replace after cycling. Traditional compressed air energy storage (CAES) systems store compressed air in caverns formed in either salt, rock, or aquifer formations (McLarnon and Cairns 1989). The requirement for specific geological features in CAES and pumped hydro make this option less attractive for remote communities and FOBs. Micro-CAES systems use smaller pressurized vessels instead of large caverns but have lower energy densities than liquid air (Ameel et al. 2013, Kim et al. 2012). Liquid air energy storage is still considered a developing technology, although, the components that make up this system are widely used in industry and are proven reliable and mature systems (Luo et al. 2015). Figure 1 depicts a top-level system diagram of how a LAES system interacts with external systems like renewable energy sources and the microgrid. Renewable energy sources like solar and wind provide necessary power to the liquefaction subsystem, where the liquid air is the fuel for energy production, which provides the needed electricity to the microgrid.

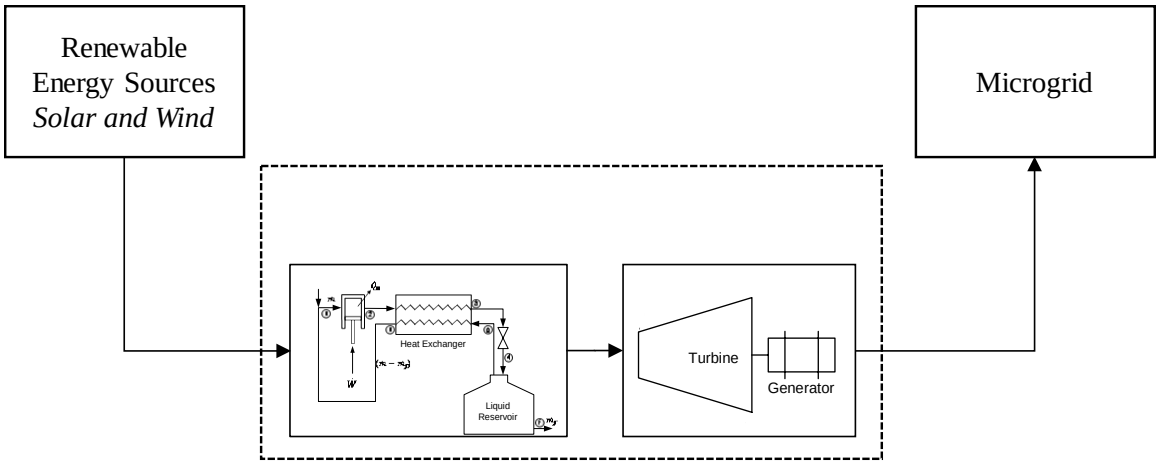

Figure 1. System Level Diagram of a LAES System.

The simplest method of liquefying air is the Linde-Hampson cycle, which consists of a compressor, two-stream heat exchanger, and a Joule Thomson (JT) valve (Hands 1986). The Linde-Hampson cycle will be further discussed in the following chapter. Additional methods include dual pressure Linde cycle, precooled Linde-Hampson cycle, Claude cycle, Kaptiza system, Heylandt cycle, and other variations (Hands 1986, Barron 1985). Liquid air is stored at 79 K in an unpressurized and insulated vessel for use during periods of intermittency (Gökçeer, Demirkaya, and Padilla 2017). In the electrical generation subsystem of LAES, liquid air is released from the storage tank where it is evaporated and expanded through a turbine to generate electricity (Gökçeer, Demirkaya, and Padilla 2017).

C. THESIS OVERVIEW

This thesis uses the manuscript option, namely using two papers submitted for publication as the core content. The previous sections introduced the motivation, background, and introduction to LAES systems. Chapter II presents a description of the components and system dynamics of the current LAES system belonging to the Naval Postgraduate School (NPS). Chapters III and IV present exact copies of two journal articles submitted to *Energy* and *Entropy*. The intent of the thesis and two papers are to act as tools in the system conceptualization stage of the V-model. The V-model is a systems engineering process used to guide the design, development, test of a system which was

"developed by NASA as part of the Software Management and Assurance Program (SMAP)" (Forsberg and Mooz 1992, 37). The decomposition and definition process focuses on "the movement from an operational need to system-level requirements" to specifications for components in the detailed design (Buede 2009, 11). The process ends with an integration and verification sequence by verifying components, subsystems, the full system through testing (Blanchard and Fabrycky 2010). Both USMC and US Army state they have a need to decrease resource demand and expand resource supply. Liquid air energy storage is a system that supports this operational need. This thesis provides tools a systems engineer may use to assist in system conceptualization to the development of system requirements. Figure 2 provides an illustrative example of where the work of this thesis fits into the V-model.

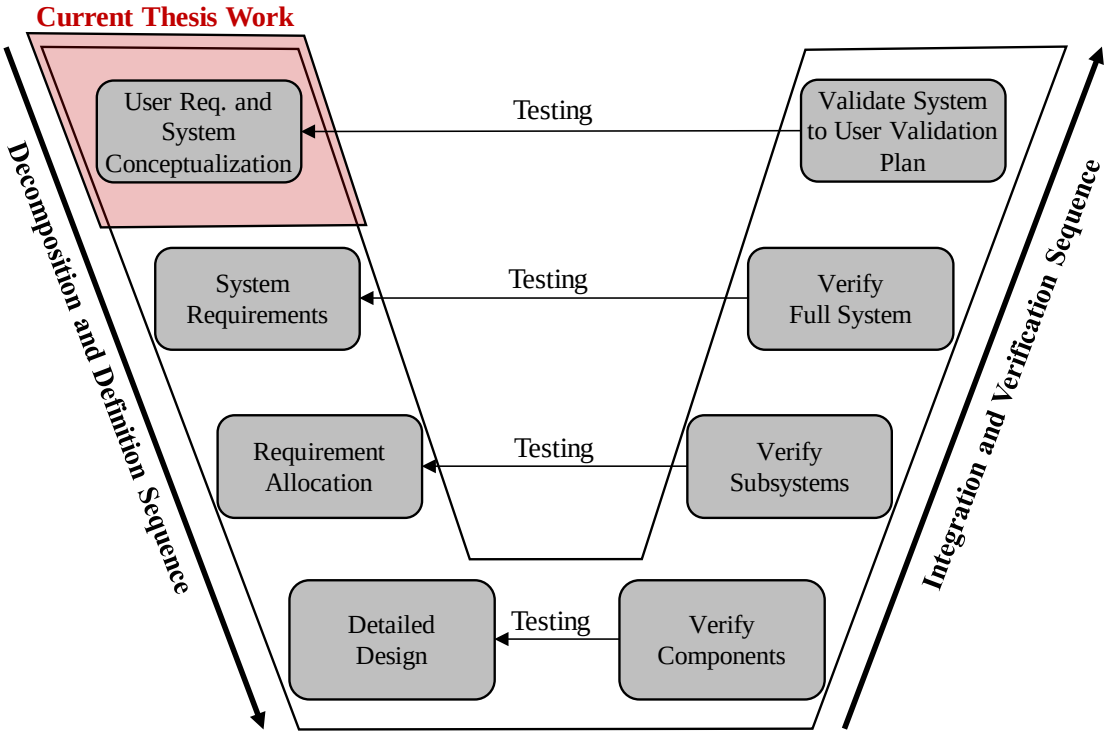

Figure 2. V-Model Example Showing Where Current Thesis is Targeted. Adapted from Blanchard and Fabrycky (2010) and Forsberg and Mooz (1992).

It is critical for systems engineers to have a basic understanding of the dynamics of a LAES system if they are to undertake the design and development of the system. The dynamics of the system is defined based on the fluid characteristics at the inlet and exit of each component of the LAES system. This unique system involves subject areas of physics, thermodynamics, and cryogenics. Although a detailed understanding of these subjects are not necessary, it is beneficial for a systems engineer to have the basic understanding of physics and thermodynamics. This thesis does not present thorough background information on these subjects and assumes the reader has a basic understanding.

The step following this thesis is modeling and simulation of a liquid air energy storage system. The results from this thesis will provide the necessary physical understanding to validate the model and simulation. The two papers presented in this thesis are titled "Closed-Form Thermodynamic Analysis of a Modified Linde-Hampson System with Binary Mixtures" and "Operating Range for an Ideal Building-Scale LAES System through Energy and Exergy Analysis."

The first paper, contained in Chapter III, presents a closed-form method of calculating the compressor work for a modified simple Linde-Hampson system and liquid yield of a binary mixture of nitrogen and oxygen using only their respective pure fluid tables. This work is important to the systems engineering process for the development of the LAES system because it provides a methodology of holistically checking a vast amount of different binary mixtures. Air is composed of mostly nitrogen and oxygen, approximately 78.10% and 20.95%, respectively (Lemmon et al. 2000). Due to the large percentages of these two gases, air is similar to a binary mixture. This paper provides a tool for studying alternative working fluids to air toward an analysis of alternatives in a trade-off study.

The second paper, contained in Chapter IV, presents an energy and exergy analysis of a liquid air energy storage system in order to identify optimum operating ranges. This paper analyzes the simple and pre-cooled Linde-Hampson liquefaction subsystems and the direct expansion method with and without heating liquid air beyond ambient temperatures in the energy production subsystem. The usefulness of this paper to systems engineers is

not only in providing an understanding of the physics and thermodynamics of the system, but in presenting a methodology to use for analyzing alternative system designs. The fundamental analysis presented in this paper provides necessary validation of future modeling and simulation.

Chapter V introduces an Excel add-in developed during this thesis work, which was vital to the analysis conducted in Chapter III. The add-in, called NIST Caddie, provides users the ability to download up to 1,048,576 rows (limit of an Excel worksheet) of fluid chemistry data from the National Institute of Standards and Technology (NIST) website. The thesis closes with conclusions and a description of future work in Chapter VI. Appendix A includes the nomenclature used for each paper. Appendix B includes the complete Visual Basic for Applications (VBA) coding for the NIST Caddie.

II. CURRENT LIQUID AIR ENERGY STORAGE SYSTEM OF INTEREST

A. SYSTEM DESCRIPTION

In 2015, the Office of Naval Research (ONR) sponsored construction of a LAES demonstration system through the Naval Facilities Engineering Command (NAVFAC) Engineering and Expeditionary Warfare Center. Nitro-Turbodyne, Inc. built this system and the Naval Postgraduate School now has possession of the system. The system was unsuccessful in producing adequate amounts of liquid air. The fundamental analysis conducted within this thesis provides the necessary understanding into the physics of the system, which may provide the insight into why this demonstration system was unsuccessful in producing liquid air. Figure 3 provides a schematic of the critical components of the Nitro-Turbodyne LAES system.

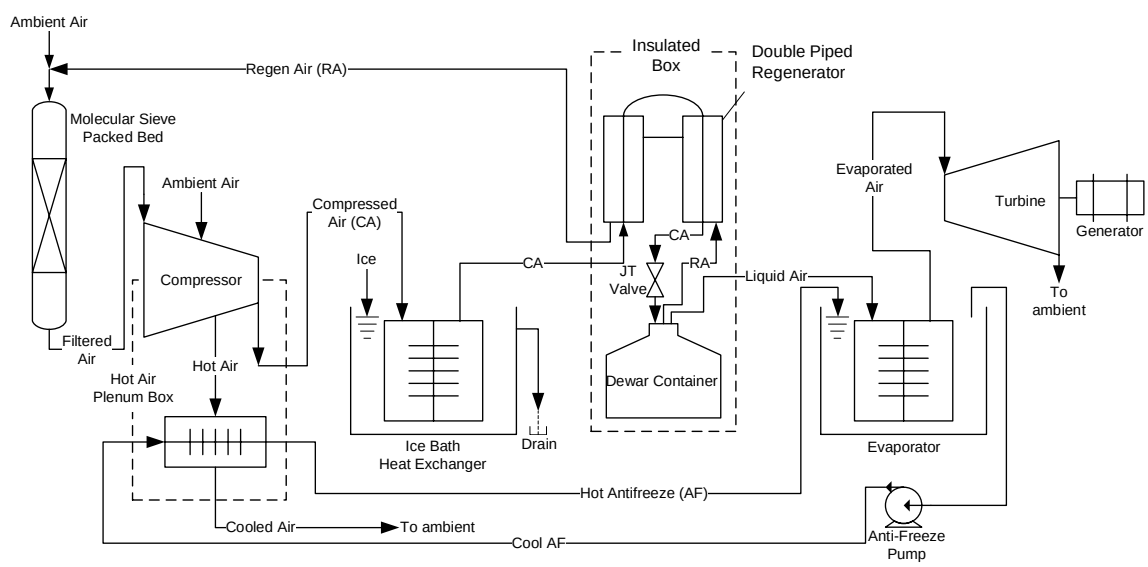

Figure 3. Schematic of the Nitro-Turbodyne, Inc. LAES System. Adapted from Nitro-Turbodyne (2016).

The liquefaction subsystem consists of a molecular sieve, a compressor, an ice water heat exchanger, a double-piped regenerator (heat exchanger), a JT valve, and a

Dewar. The molecular sieve removes moisture and CO_2 from ambient air by using a mixture of sorbent 4A and sorbent 13X (Nitro-Turbodyne 2016). The removal of water and CO_2 from the system eliminates the concern for the fluids freezing since water freezes at 273.15 K and CO_2 freezes at 194.75 K (Lemmon, McLinden, and Friend n.d.). What remains is 78.12% nitrogen, 20.96% oxygen, and 0.92% Argon (Lemmon et al. 2000). Figure 4 shows an image of the molecular sieve, otherwise known as the air intake scrubber.

Figure 4. Image of the Molecular Sieve as Part of the Nitro-Turbodyne, Inc. LAES System. Adapted from Nitro-Turbodyne (2016).

The compressor is a commercial-off-the-shelf (COTS) compressor made by Airtex, as depicted in Figure 5. The compressor is capable of producing up to 3.5 ft^3 per min. at about 4500 psi. The ice-bath heat exchanger's purpose is to reduce the temperature of the fluid exiting the compressor. It cools the air via a finned heat exchanger in an ice water bath, as shown in Figure 6.

The double-piped heat exchanger, JT valve, and Dewar are a part of the condenser subsystem, as shown in Figure 7. The double-piped heat exchanger is a cross-flow heat exchanger with a high-pressure stainless steel hose line inside of a larger atmospheric

Figure 5. Image of the Compressor as Part of the Nitro-Turbodyne, Inc. LAES System. Source: Nitro-Turbodyne (2016).

Figure 6. Image of the Ice-Bath Heat Exchanger as Part of the Nitro-Turbodyne, Inc. LAES System. Source: Nitro-Turbodyne (2016).

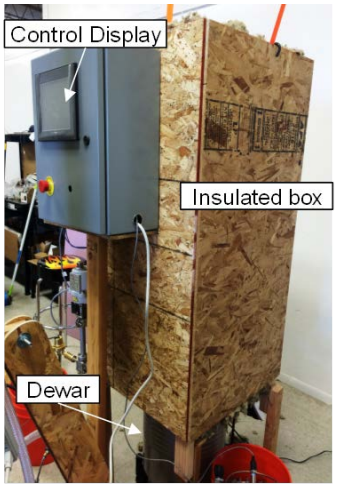

Figure 7. Image of the Condenser Subsystem as Part of the Nitro-Turbodyne, Inc. LAES System. Adapted from Nitro-Turbodyne (2016).

pressure rubber corrugated hose. The double-piped heat exchanger's purpose is to cool the incoming air prior to reaching the JT valve. The JT valve is a pressure-reducing device, which maintains a constant enthalpy of the air as it passes through. The double-piped heat exchanger and JT valve are within the insulated box. The final component of the liquefaction subsystem is the Dewar, which stores liquid air at approximately 79 K.

The electrical generation subsystem consists of an evaporator, an anti-freeze subsystem, turbine, and generator. The evaporator is similar to the ice-bucket heat exchanger except instead of ice water the bucket contains hot anti-freeze. The anti-freeze subsystem acts as a thermal energy storage system. It captures the heat rejected from the compressor via a finned heat exchanger, uses the hot anti-freeze to heat the liquid air in the evaporator, and then cycled back to the compressor by the anti-freeze pump. The turbine and generator receive the high-pressure evaporated air generating electricity. The control box displays information from multiple sensors that are reading pressure, temperature, flow rate, and such, from sensors throughout the system.

B. SYSTEM DYNAMICS

Figure 8 is a block diagram of the Nitro-Turbodyne, Inc. The LAES system and serves as a tool to explain its system dynamics. This system takes in ambient air first through the molecular sieve. As stated previously, the molecular sieve removes the moisture and CO_2 from ambient air. This filtered air then enters the compressor, where the air is compressed from atmospheric pressure to 250 atmospheres (atm). As pressure increases, the temperature increases as well. The compressor is a three-stage compressor. It sequentially compresses air in each stage and cooled via convection from fins and a cooling fan. According to the manufacturer, the compressor is capable of rejecting enough heat so that the compressed air is less than 10°F above ambient temperature (Airetex 2006). The anti-freeze heat exchanger captures the heat rejected from the compressor and transfers the resulting hot anti-freeze to later components in the system. The ice-bath heat exchanger next receives the compressed air and cools it to ambient temperature or below. Next, the double-piped heat exchanger receives the compressed air and transfers to the JT valve. The JT valve reduces the pressure from 250 atm to just above ambient pressure. During this

pressure reduction, the temperature drops significantly. If the temperature of the compressed air into the JT valve is low enough, the output of the JT valve will be a mixture of liquid and gaseous air. The liquid air is stored in the Dewar until it is ready to be used and the remaining gaseous air (or regen air) is returned to the double-piped heat exchanger. As Figure 3 shows, the regen air then cools the incoming compressed air prior to it entering the JT valve and finally returns to the molecular sieve. Theoretically, this system requires approximately 180 minutes from a "cold start" to generate liquid air. Although, ONR reported this system was not successful in generating liquid air.

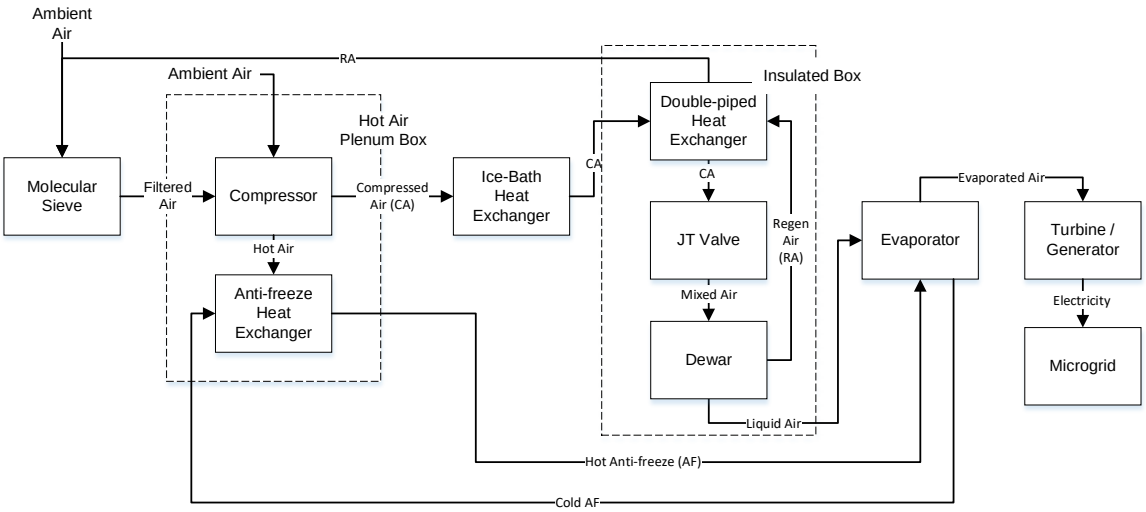

Figure 8. Block Diagram of Nitro-Turbodyne, Inc. LAES System

The required temperature of air to become a liquid is 78.9 K (Lemmon et al. 2000). Air undergoes a throttling process as it passes through the JT valve. In a throttling process, the enthalpy does not change, but the pressure drops and temperature either drops or increases (Moran and Shapiro 2004, 549–550). The required temperature of air entering the JT valve can be determined by referencing the enthalpy of air at 78.9 K and at atmospheric pressure and then referencing the same enthalpy at the incoming pressure. For example, if the incoming pressure is approximately 200 atm and the exit pressure is 1 atm, the enthalpy at 78.9 K is approximately 79.21 kJ/kg. Therefore, at 200 atm, the approximate temperature of air entering the JT valve must be 178.3 K. Due to the requirement of this

low temperature, the system must cycle through the liquefaction subsystem many times before the air is cool enough prior to entering the JT valve in order to generate liquid air.

Once an adequate amount of liquid air has been created and there is a system demand for additional electricity, the Dewar releases liquid air to the electrical generation subsystem. The evaporator receives the liquid air. The hot antifreeze bath in the evaporator heats the liquid air back to a gas at roughly room temperature. Due to the design of this system, the pressure maintains at just above ambient, but the kinetic energy in the gas increases. This is because the volume of one kilogram of liquid air is $1.154 \times 10^{-3} m^3$ and the volume of one kilogram of gaseous air at room temperature is $0.835 m^3$ (Bell 1963). This is an increase of over 700 times the volume of liquid air. The expansion of air is constrained to a constant diameter stainless steel tube, and therefore, the velocity of the air increases accordingly. Due to NPS not having possession of the turbine for this system, it is assumed that an impulse or reaction turbine spins due to the high velocity of the air. This in turn spins the generator, which creates electricity for any use such as for a microgrid or for base camp operations.

III. PAPER I: CLOSED-FORM THERMODYNAMIC ANALYSIS OF A MODIFIED LINDE-HAMPSON SYSTEM WITH BINARY MIXTURES

This chapter has been submitted for publication in a journal by the authors Todd A. Howe, Anthony G. Pollman, and Anthony J. Gannon.

A. ABSTRACT

This paper presents a closed-form method of calculating the compressor work for a modified simple Linde-Hampson system and liquid yield of a binary mixture of nitrogen and oxygen using only their respective pure fluid tables. The modified system uses two compressors in lieu of a single compressor, one compressor for makeup gas and a second for return gas. The methodology presented can be used for any non-reacting binary mixture of liquefaction fluids at any composition and for analysis with alternative liquefaction systems. The two-compressor model yields more conservative results than the single compressor model but is a useful alternative when detailed experimental data of a binary mixture is not available. This work is a part of a larger study for the design of a small-scale liquid air energy storage (LAES) system. The analytical approach presented in this paper for a binary mixture of nitrogen and oxygen provide the means to validate future modeling of cryogenic systems based on different binary working fluids.

Keywords: energy storage, cryogenic, binary mixture, liquefaction systems, liquid air

B. INTRODUCTION

Patented in the 1903, the Linde-Hampson (LH) liquefaction system shown in Figure 9 was the second system used to liquefy gases and is the simplest of all liquefaction systems (Barron 1985, Hands 1986, Bell 1963, Linde 1903). This paper will first introduce the analysis of this system for a single pure fluid and then the analysis for a binary fluid mixture.

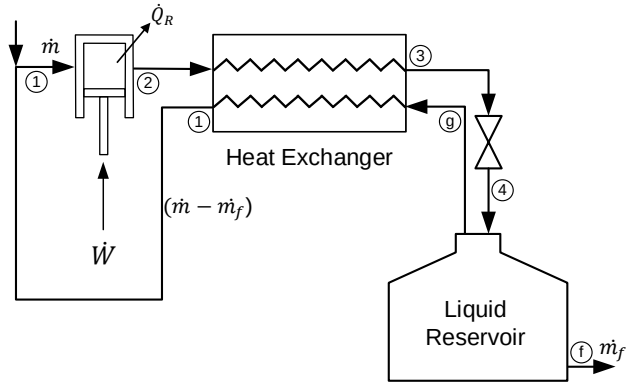

Figure 9. Simple Linde-Hampson Liquefaction System. Adapted from Barron (1985).

As shown in Figure 9, at steady state, the pure fluid at ambient conditions is isothermally compressed (1 to 2) and precooled through the heat exchanger (3). Next, the fluid goes through a throttling process through the Joule Thomson (JT) valve where it becomes a two-phase mixture (4). The liquid generated remains in a reservoir and the gas cycles back through the heat exchanger, cooling the gas from state 2 to 3, and returns to the compressor at state 1 condition. The mass flow rate of the liquid gas is equal to the mass flow rate of the makeup gas.

The temperature-entropy diagram (T-s) shown in Figure 10 provides an example of how the states change within the simple Linde-Hampson system for nitrogen as the working fluid. An example of a thermodynamically ideal liquefaction system is presented as dashed lines in Figure 10. In this ideal system, gas is isothermally compressed from state 1 to 2 and undergoes isentropic expansion from state 2 to f at the initial pressure of state 1 (Barron 1985). The thermodynamically ideal liquefaction system is used to compare the system when using different fluids through a figure of merit (FOM) (Barron 1985).

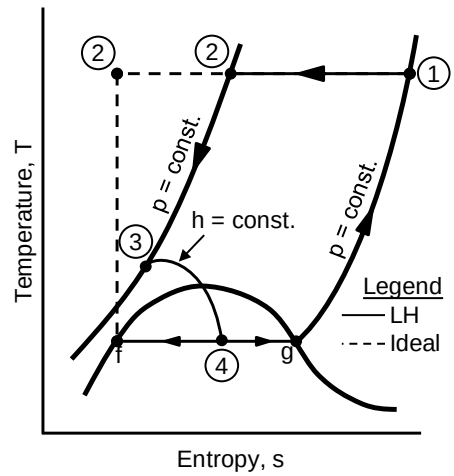

Figure 10. Diagram of Simple Linde-Hampson Cycle. Adapted from Barron (1985).

C. SIMPLE LINDE-HAMPSON SYSTEM ANALYSIS

The simplest way to conduct a thermodynamic analysis on this system is two draw two control volumes, one around the compressor and the second around the heat exchanger, JT valve, and liquid reservoir (Barron 1985). Using the first and second law for the compressor (Barron 1985, Moran and Shapiro 2004)

$$\dot{Q}_R + \dot{m}h_1 = \dot{m}h_2 + \dot{W}_c \rightarrow \frac{\dot{W}_c}{\dot{m}} = \frac{\dot{Q}_R}{\dot{m}} + (h_2 - h_1) \qquad (1)$$

$$\dot{m}s_2 = \dot{m}s_1 + \frac{\dot{Q}_R}{T_1} \rightarrow \frac{\dot{Q}_R}{\dot{m}} = T_1(s_2 - s_1)\ . \qquad (2)$$

Combining equations (1) and (2) to get specific work or work per unit mass compressed (Barron 1985).

$$\frac{\dot{W}_c}{\dot{m}} = T_1(s_1 - s_2) + (h_2 - h_1) \qquad (3)$$

For the thermodynamically ideal liquefaction system, the work per unit mass compressed is equal to the work per unit mass liquefied because 100 percent of the gas compressed is liquefied (Barron 1985).

$$\frac{\dot{W}_i}{\dot{m}} = T_1(s_1 - s_f) + (h_f - h_1) = \frac{\dot{W}_i}{\dot{m}_f} \tag{4}$$

For the second control volume, there is no work or heat transferred to or from the control volume; therefore, the first law reduces to (Barron 1985).

$$\dot{m}h_2 = \dot{m}_f h_f + (\dot{m} - \dot{m}_f)h_1 \tag{5}$$

Solving for the fraction of the liquid mass flow rate will give the liquid yield, defined as Y (Barron 1985).

$$Y = \frac{\dot{m}_f}{\dot{m}} = \frac{h_2 - h_1}{h_f - h_1} \tag{6}$$

The final system performance is the work required for liquefaction. Substituting Equation (5) into (3) gives the work per unit mass liquefied (Barron 1985).

$$\frac{\dot{W}_c}{\dot{m}_f} = \frac{\dot{W}_C}{\dot{m}Y} = [T_1(s_1 - s_2) + (h_2 - h_1)]\left(\frac{h_f - h_1}{h_2 - h_1}\right) \tag{7}$$

The figure of merit is defined as

$$FOM = \frac{\dot{W}_i}{\dot{m}_f} / \frac{\dot{W}_c}{\dot{m}_f}. \tag{8}$$

shows the performance of the Linde-Hampson cycle using a temperature of $T_1 = T_2 = 300K$ and pressures of $p_1 = 1$ atm and $p_2 = 200$ atm for pure nitrogen, oxygen, and air (Barron 1985). This table presents results from Baron and results from the previous equations using available fluid tables from NIST and Lemmon.

Table 1. Performance of the Linde-Hampson Cycle.

Fluid	Liquid Yield (Y)	Work/Unit Mass Compressed (kJ/kg)	Work/Unit Mass Liquefied (kJ/kg)	Figure of Merit	Source
N_2	0.0708	472.5	6673	0.1151	(Barron 1985, 74)
O_2	0.1065	405.0	3804	0.1671	(Barron 1985, 74)
Air	0.0808	454.1	5621	0.1313	(Barron 1985, 74)
N_2	0.0746	472.8	6335	0.1214	(Lemmon, McLinden, and Friend n.d.)
O_2	0.1063	405.9	3819	0.1663	(Lemmon, McLinden, and Friend n.d.)
Air	0.0808	453.9	5622	0.1316	(Lemmon et al. 2000)

The analysis of the Linde-Hampson system with a binary mixture as the working fluid is different from a single pure substance. Using a control volume round the heat exchanger, JT-valve and liquid reservoir, conservation of mass shows

$$\dot{m}_2 = \dot{m}_1 + \dot{m}_f \tag{9}$$

and

$$\dot{m}_1 = \dot{m}_g. \tag{10}$$

The first law energy balance is

$$\begin{aligned} &\dot{m}_{f_{N_2}} h_{2_{N_2}} + \dot{m}_{fO_2} h_{2_{O_2}} + \dot{m}_{g_{N_2}} h_{2_{N_2}} + \dot{m}_{g_{O_2}} h_{2_{O_2}} = \\ &\dot{m}_{f_{N_2}} h_{f_{N_2}} + \dot{m}_{f_{O_2}} h_{f_{O_2}} + \dot{m}_{g_{N_2}} h_{1_{N_2}} + \dot{m}_{g_{O_2}} h_{1_{O_2}} \end{aligned} \tag{11}$$

The individual mass flow rates are unknown, and therefore, more information is needed to determine the yield and work. A vapor liquid equilibrium (VLE) diagram for oxygen and nitrogen will provide the molar fraction of oxygen and nitrogen in liquid and vapor phases. According to Raoult's Law, the partial pressure of a substance is the product of its vapor pressure and its mole fraction in the mixture (Barron 1985).

$$p_j = \pi_j x_j \tag{12}$$

Where the partial pressure of is p_j, the vapor pressure is π_j, and the liquid molar fraction is x_j. Assuming the gaseous mixture behaves as an ideal gas, the total pressure of the mixture based on the Gibbs-Dalton Law is (Gillespie 1930)

$$p_j = py_j, \tag{13}$$

where y_j is the vapor mole fraction of the jth component in the mixture. Combining equations 12 and 13 gives

$$y_j = (\pi_j/p)x_j, \tag{14}$$

Assuming that the gas is ideal and the liquid is a perfect mixture, the total pressure is (Barron 1985)

$$p = \sum_j p_j = \sum_j \pi_j x_j. \tag{15}$$

A binary mixture like oxygen and nitrogen therefore has a total pressure of

$$p = \pi_{O_2} x_{O_2} + \pi_{N_2}(1 - x_{O_2}). \tag{16}$$

The point at which nitrogen and oxygen are a two phase mixture is immediately following the JT valve and inside the liquid reservoir. Using a total pressure of the mixture inside the liquid reservoir as one atmosphere, the resulting temperature-composition diagram for an oxygen-nitrogen mixture is shown in Figure 11. Partial pressures for oxygen and nitrogen were taken from NIST tables (Lemmon, McLinden, and Friend n.d.). Figure 11 shows the progression of the mixture from initial operation to steady state; where the mole fraction of gaseous and liquid oxygen and nitrogen is 0.213 and 0.787, respectively.

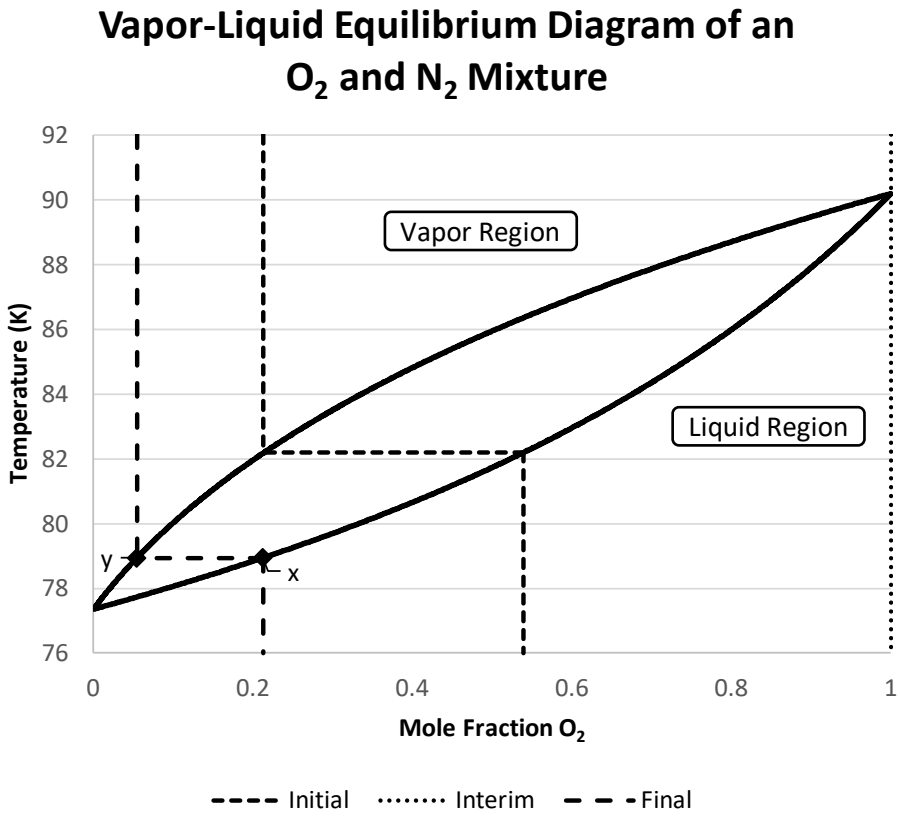

Figure 11. VLE Diagram of an Oxygen and Nitrogen Mixture

The final temperature where equilibrium was achieved using the partial pressures from the NIST tables was 78.943 K. This differs slightly from Lemmon's temperature of 78.903 K for liquid air (Lemmon et al. 2000).

The composition of oxygen and nitrogen gases returning to the heat exchanger and compressor is at the equilibrium temperature. The composition of oxygen and nitrogen gases entering the heat exchanger from the compressor is still not known due to the mixing of makeup air. Therefore, a closed-form solution can be found by the addition of a second compressor, and thus modifying the current Linde-Hampson system.

D. MODIFIED LH SYSTEM WITH A BINARY MIXTURE

The modified Linde-Hampson system has two compressors, one compressor for makeup air and a second compressor for the returning gas. Figure 12 displays the modified system with new state numbers.

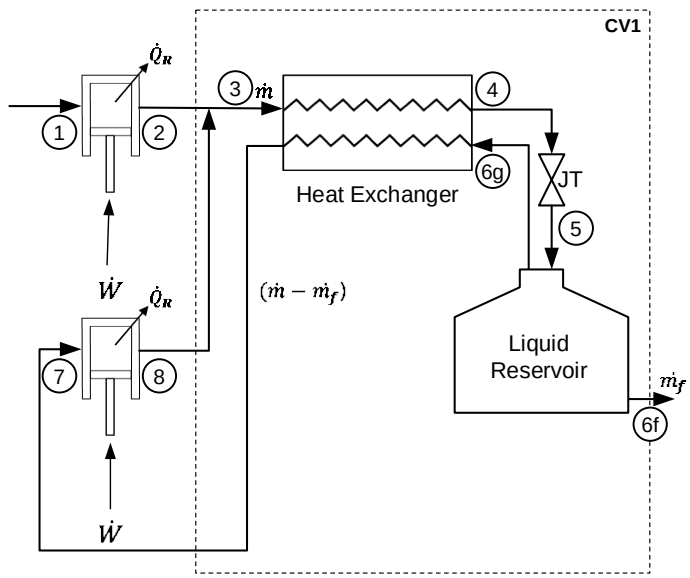

Figure 12. Modified Linde-Hampson System with Two Compressors.

At steady state, the composition of liquid nitrogen and oxygen generated is equivalent to the composition of nitrogen and oxygen gas entering into the system as makeup gas. The initial vapor and final liquid lines in Figure 11 also shows this. After converting the molar fraction of nitrogen and oxygen to a mass fraction, the composition liquid nitrogen and oxygen is defined as

$$\frac{\dot{m}_{f_{O_2}}}{\dot{m}_{f_{N_2}}} = x, \tag{17}$$

and the composition of gaseous nitrogen and oxygen returning back to the second compressor is

$$\frac{\dot{m}_{g_{O_2}}}{\dot{m}_{g_{N_2}}} = y. \tag{18}$$

The liquid yield of the system is the ratio of the liquid mass flow rate to the overall mass flow rate

$$Y = \frac{\dot{m}_f}{\dot{m}} = \frac{\dot{m}_{f_{N_2}} + \dot{m}_{f_{O_2}}}{\dot{m}_{f_{N_2}} + \dot{m}_{f_{O_2}} + \dot{m}_{g_{N_2}} + \dot{m}_{g_{O_2}}}. \tag{19}$$

Substituting oxygen terms for nitrogen terms from equations (17) and (18) gives

$$Y = \frac{\dot{m}_{f_{N_2}}(1+x)}{\dot{m}_{f_{N_2}}(1+x) + \dot{m}_{g_{N_2}}(1+y)}. \tag{20}$$

Rearranging terms results in

$$Y = \frac{1}{1 + \frac{\dot{m}_{g_{N_2}}(1+y)}{\dot{m}_{f_{N_2}}(1+x)}} \ . \tag{21}$$

The first law energy balance for the modified system within control volume 1 is

$$\begin{aligned} &\dot{m}_{f_{N_2}} h_{2_{N_2}} + \dot{m}_{f_{O_2}} h_{2_{O_2}} + \dot{m}_{g_{N_2}} h_{8_{N_2}} + \dot{m}_{g_{O_2}} h_{8_{O_2}} = \\ &\dot{m}_{f_{N_2}} h_{6f_{N_2}} + \dot{m}_{f_{O_2}} h_{6f_{O_2}} + \dot{m}_{g_{N_2}} h_{7_{N_2}} + \dot{m}_{g_{O_2}} h_{7_{O_2}} \end{aligned} \ . \tag{22}$$

Substituting oxygen terms for nitrogen terms from equations (17) and (18) gives

$$\begin{aligned} &\dot{m}_{f_{N_2}} h_{2_{N_2}} + x\dot{m}_{f_{N_2}} h_{2_{O_2}} + \dot{m}_{g_{N_2}} h_{8_{N_2}} + y\dot{m}_{g_{N_2}} h_{8_{O_2}} = \\ &\dot{m}_{f_{N_2}} h_{6f_{N_2}} + x\dot{m}_{f_{N_2}} h_{6f_{O_2}} + \dot{m}_{g_{N_2}} h_{7_{N_2}} + y\dot{m}_{g_{N_2}} h_{7_{O_2}} \end{aligned} \ . \tag{23}$$

Dividing both sides by $\dot{m}_{f_{N_2}}$ and reducing results in

$$\frac{\dot{m}_{g_{N_2}}}{\dot{m}_{f_{N_2}}} = \frac{h_{6f_{N_2}} - h_{2_{N_2}} + x\left(h_{6f_{O_2}} - h_{2_{O_2}}\right)}{h_{8_{N_2}} - h_{7_{N_2}} + y\left(h_{8_{O_2}} - h_{7_{O_2}}\right)} \ . \tag{24}$$

Substituting Equation 24 into 21 results in a final yield equation of

$$Y = 1 \Big/ \left(1 + \frac{h_{6f_{N_2}} - h_{2_{N_2}} + x\left(h_{6f_{O_2}} - h_{2_{O_2}}\right)(1+y)}{h_{8_{N_2}} - h_{7_{N_2}} + y\left(h_{8_{O_2}} - h_{7_{O_2}}\right)(1+x)}\right) \ . \tag{25}$$

The compressor work is in terms of total mass flow rate. Therefore, an equation to relate the mass flow rate of liquid and gaseous nitrogen and oxygen to total mass flow rate is required. This is achieved using equations (17), (18), and (19) to write each mass flow component in terms of the total mass flow, yield and mass fractions x and y.

$$\dot{m}_{f_{N_2}} = \frac{\dot{m}Y}{(1+x)} \tag{26}$$

$$\dot{m}_{f_{O_2}} = \frac{x\dot{m}Y}{(1+x)} \tag{27}$$

$$\dot{m}_{g_{N_2}} = \frac{\dot{m}(1-Y)}{(1+y)} \tag{28}$$

$$\dot{m}_{g_{O_2}} = \frac{y\dot{m}(1-Y)}{(1+y)} \tag{29}$$

The compressor has a work per unit mass compressed based on the first and second law equations. The first law and second equation for the makeup air compressor is (compressor 1)

$$\dot{W}_{c_1} = \dot{Q}_{R_1} + \dot{m}_{f_{N_2}}\left(h_{2_{N_2}} - h_{1_{N_2}}\right) + \dot{m}_{f_{O_2}}\left(h_{2_{O_2}} - h_{1_{O_2}}\right) \tag{30}$$

$$\dot{Q}_{R_1} = T_1\left[\dot{m}_{f_{N_2}}\left(s_{2_{N_2}} - s_{1_{N_2}}\right) + \dot{m}_{f_{O_2}}\left(s_{2_{O_2}} - s_{1_{O_2}}\right)\right] \quad . \tag{31}$$

Substituting in equations (26) and (27)

$$\dot{W}_{c_1} = \dot{Q}_{R_1} + \frac{\dot{m}Y}{(1+x)}\left(h_{2_{N_2}} - h_{1_{N_2}}\right) + \frac{x\dot{m}Y}{(1+x)}\left(h_{2_{O_2}} - h_{1_{O_2}}\right) \tag{32}$$

$$\dot{Q}_{R_1} = T_1\left[\frac{\dot{m}Y}{(1+x)}\left(s_{2_{N_2}} - s_{1_{N_2}}\right) + \frac{x\dot{m}Y}{(1+x)}\left(s_{2_{O_2}} - s_{1_{O_2}}\right)\right] \quad . \tag{33}$$

Combining equations (32) and (33) and dividing through by mass flow rate yields the compressor work per unit mass

$$\frac{\dot{W}_{c_1}}{\dot{m}} = T_1\left[\frac{Y}{(1+x)}\left(s_{2_{N_2}} - s_{1_{N_2}}\right) + \frac{xY}{(1+x)}\left(s_{2_{O_2}} - s_{1_{O_2}}\right)\right] +$$

$$\frac{Y}{(1+x)}\left(h_{2_{N_2}} - h_{1_{N_2}}\right) + \frac{xY}{(1+x)}\left(h_{2_{O_2}} - h_{1_{O_2}}\right) \ . \tag{34}$$

The compressor work per unit mass for the return air (compressor 2) is therefore

$$\frac{\dot{W}_{c_2}}{\dot{m}} = T_1\left[\frac{Y}{(1+x)}\left(s_{8_{N_2}} - s_{7_{N_2}}\right) + \frac{xY}{(1+x)}\left(s_{8_{O_2}} - s_{7_{O_2}}\right)\right] + \frac{Y}{(1+x)}\left(h_{8_{N_2}} - h_{7_{N_2}}\right) + \frac{xY}{(1+x)}\left(h_{8_{O_2}} - h_{7_{O_2}}\right) \ . \tag{35}$$

The total compressor work for the system is the sum of equations (34) and (35).

$$\frac{\dot{W}_c}{\dot{m}} = \frac{\dot{W}_{c_1}}{\dot{m}} + \frac{\dot{W}_{c_2}}{\dot{m}} \tag{36}$$

The calculation for compressor work per unit mass liquefied is simply the work per unit mass divided by the liquid yield.

$$\frac{\dot{W}_c}{\dot{m}_f} = \frac{\dot{W}_c}{\dot{m}Y} \tag{37}$$

The ideal compression work for this modified system is calculated using states 1 and 6f, using a modified form of Equation (4).

$$\dot{W}_{C_i} = \dot{Q}_{R_i} + \dot{m}_{f_{N_2}}\left(h_{6f_{N_2}} - h_{1_{N_2}}\right) + \dot{m}_{f_{O_2}}\left(h_{6f_{O_2}} - h_{1_{O_2}}\right) \tag{38}$$

$$\dot{Q}_{R_i} = T_1\left[\dot{m}_{f_{N_2}}\left(s_{1_{N_2}} - s_{6f_{N_2}}\right) + \dot{m}_{f_{O_2}}\left(s_{1_{O_2}} - s_{6f_{O_2}}\right)\right] \tag{39}$$

Substituting Equation (39) into (38) and substituting mass flow rates with equations (26) and (27) yields

$$\dot{W}_{C_i} = T_1\left[\frac{\dot{m}Y}{(1+x)}\left(s_{1_{N_2}} - s_{6f_{N_2}}\right) + \frac{x\dot{m}Y}{(1+x)}\left(s_{1_{O_2}} - s_{6f_{O_2}}\right)\right] + \frac{\dot{m}Y}{(1+x)}\left(h_{6f_{N_2}} - h_{1_{N_2}}\right) + \frac{x\dot{m}Y}{(1+x)}\left(h_{6f_{O_2}} - h_{1_{O_2}}\right) \ , \tag{40}$$

resulting in an ideal compressor work per unit mass liquefied of

$$\frac{\dot{W}_{C_i}}{\dot{m}Y} = \frac{\dot{W}_{C_i}}{\dot{m}_f} = T_1\left[\frac{\left(s_{1_{N_2}} - s_{6f_{N_2}}\right)}{(1+x)} + \frac{x\left(s_{1_{O_2}} - s_{6f_{O_2}}\right)}{(1+x)}\right] +$$

$$\frac{\left(h_{6f_{N_2}}-h_{1_{N_2}}\right)}{(1+x)}+\frac{x\left(h_{6f_{O_2}}-h_{1_{O_2}}\right)}{(1+x)} \ . \qquad (41)$$

E. RESULTS AND DISCUSSION

The system is assumed to be operating at two different pressures, 1 atm at states, 1 and 5 through 7 and 200 atm at states 2 through 4 and 8. The compressors are assumed to be operating isothermally. The temperature at each state is 300 K except for states 6f and 6g, which are at 78.94 K, based on the vapor-liquid equilibrium diagram. The final step to calculate the yield and work for the two-compressor Linde Hampson system is to determine the correct enthalpy and entropy values. The values found in tables are based on pure fluids, and therefore, they must be adjusted to account for compressibility in the fluids in a mixture. Some iteration is required to determine these as the partial pressures are dependent on the compressibility factors Z_i of each component. The compressibility factor of a fluid mixture is (Moran and Shapiro 2004)

$$Z = \sum y_i Z_i \,|_{T,V}, \qquad (42)$$

where y_i is the fluid mole fraction, and Z_i is the fluid compressibility factor at a constant temperature and volume. The individual fluid compressibility factor is (Moran and Shapiro 2004)

$$Z_i = \frac{p_i}{\rho_i R_i T}, \qquad (43)$$

where p_i is the real fluid gas partial pressure, ρ_i is its density, R_i is the fluid gas constant, and T is the temperature. The partial pressure of the fluid gas is

$$p_{zi} = \frac{y_i Z p}{Z_i} = \frac{p_i Z}{Z_i} \ . \qquad (44)$$

The corrected partial pressure of the fluid gas is known, and therefore, the real fluid gas partial pressure is

$$p_i = \frac{Z_i p_{zi}}{Z} \ . \qquad (45)$$

Following the previous procedures, the resulting molar fractions and real partial pressures for nitrogen and oxygen are displayed in Table 2 for states 1,2, 6f, 7, and 8.

Table 2. Molar Fractions and Partial Pressures for Nitrogen and Oxygen and Different States.

State	$\boldsymbol{T}$ **(K)**	$\boldsymbol{p}$ **(atm)**	$\boldsymbol{y_{N_2}}$	$\boldsymbol{p_{N_2}}$ **(atm)**	$\boldsymbol{y_{O_2}}$	$\boldsymbol{p_{O_2}}$ **(atm)**
1	300	1	0.787	0.786	0.213	0.214
2	300	200	0.787	159.2	0.213	40.77
8	300	200	0.945	189.6	0.055	10.37
6f	78.94	1	0.787	1.000	0.213	1.000
7	300	1	0.945	0.945	0.055	0.055

The enthalpy and entropy values for nitrogen and oxygen were collected from (Lemmon, McLinden, and Friend n.d.) according to the corresponding temperature and partial pressure shown in Table 3. Table 3 provides the resulting yield, compressor work, and figure of merit for the nitrogen and oxygen mixture.

Table 3. Results for Nitrogen and Oxygen Mixture in Modified Linde Hampson System.

Fluid	**Liq. Yield (Y)**	$\frac{\dot{W}_{c_1}}{\dot{m}}$ **(kJ/kg)**	$\frac{\dot{W}_{c_2}}{\dot{m}}$ **(kJ/kg)**	$\frac{\dot{W}_c}{\dot{m}}$ **(kJ/kg)**	$\frac{\dot{W}_c}{\dot{m}_f}$ **(kJ/kg)**	**Figure of Merit**
N_2 (.787) O_2 (.213)	0.1042	47.7	420.0	467.7	4489	0.0784

The overall work per unit mass compressed for the modified system agrees within 3% of the simple Linde-Hampson system. In addition, if the calculations presented are used to calculate the work per unit mass compressed for a pure substance of nitrogen or oxygen, the results are equivalent as shown in Table 1. Figure 13 shows the change in work per unit mass compressed as the composition of nitrogen and oxygen are varied in the modified

system. This equivalency at 100% nitrogen and 100% oxygen validates the calculations presented.

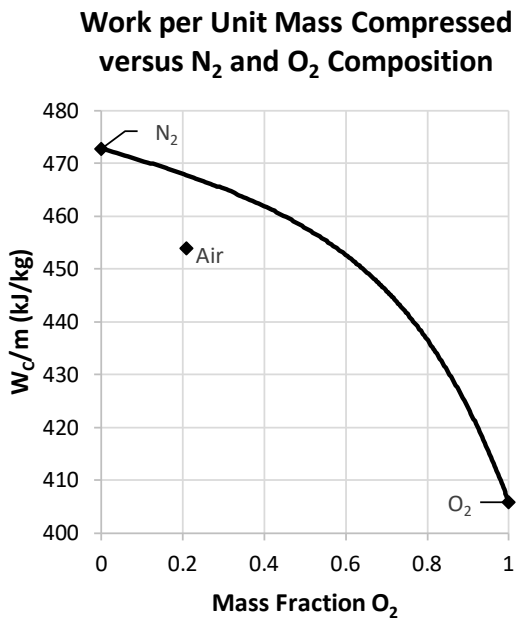

This graph shows the change in work per unit mass compressed based on the composition of nitrogen and oxygen. In addition, it shows the work for air, 100% nitrogen, and 100% oxygen based on the values presented in Table 1.

Figure 13. Composition of Nitrogen and Oxygen versus Work per Unit Mass Compressed (kJ/kg).

The yield for the modified system is significantly different due to the use of a second compressor in parallel. This difference affects the figure of merit, as shown in Figure 14. This figure may be useful when choosing a desired composition of a mixture in order to achieve optimal performance. Figures 13 and 14 also show the corresponding values for air from Barron and NIST tables.

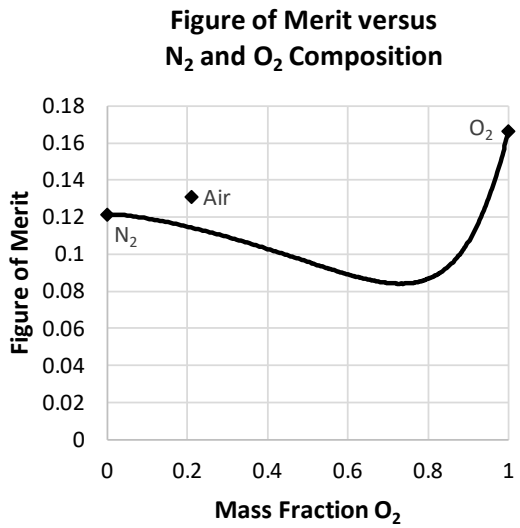

This graph shows the figure of merit based on the composition of nitrogen and oxygen. In addition, it shows the work for air, 100% nitrogen, and 100% oxygen based on the values presented in Table 1.

Figure 14. Composition of Nitrogen and Oxygen versus Figure of Merit.

The difference in the figure of merit in the two compressor model is mainly due to entropy generation in the mixing of the two high pressure streams as opposed to the mixing taking place at a low pressure before the single compressor.

F. CONCLUSIONS

This paper presented a closed-form solution to analyzing a binary mixture within a modified Linde-Hampson system. The methodology presented could be used for any non-reacting binary mixture at any composition. Although the modified Linde-Hampson system is not physically the same system as the simple Linde-Hampson system, the work per unit mass compressed for each system is equivalent when observing each substance of the binary mixture in its pure state. The modified system results in more conservative estimates of performance but is still physically realistic and useful for binary mixtures where data is only available for the individual components. Even though the liquid yield for the two systems is different, the modified system is useful for comparison of various binary mixtures. Future work includes addition of non-reacting ternary mixtures, modeling of LAES system with binary mixtures, and analysis with alternative liquefaction systems.

G. ACKNOWLEDGMENTS

This work was sponsored by ESTEP (Energy Systems Technology Evaluation Program) funded by the Office of Naval Research under the technical monitors of Richard Carlin and Marissa Brand.

IV. PAPER II: OPERATING RANGE FOR AN IDEAL BUILDING-SCALE LAES SYSTEM THROUGH ENERGY AND EXERGY ANALYSIS

This chapter has been submitted for publication in a journal by the authors Todd A. Howe, Anthony G. Pollman, and Anthony J. Gannon.

A. ABSTRACT

This paper presents an ideal energy and exergy analysis of a liquid air energy storage (LAES) system to identify optimum operating points within the system. This system uses the simple Linde-Hampson and pre-cooled Linde-Hampson cycles for the liquefaction subsystem and direct expansion method with and without heating above ambient temperature for the energy production subsystem. This work presents the upper bounds of energy and exergetic efficiency for the LAES system; presents the effectiveness of pre-cooling air for liquefaction and heating air beyond ambient temperature for energy production; and analysis on the components of the LAES system. This work is a part of a larger study for the design of a building-scale LAES system. The analytical approach presented in this paper may be applied to other LAES configurations to identify optimal operating points of the system energy and exergetic efficiencies.

Keywords: liquid air energy storage, energy analysis, exergy analysis, cryogenic system

B. INTRODUCTION

Liquid air energy storage (LAES) is a developing thermal electrical energy storage technology and is a promising addition to other long-term storage technologies such as pumped hydroelectric storage (PHS) and compressed air energy storage (CAES) (Luo et al. 2015, Chen et al. 2009). LAES has a higher energy density than PHS and four to six times the energy density of CAES at 200 bar (Luo et al. 2015, Wang et al. 2015). Studies have shown LAES is capable of higher round trip efficiency than CAES (Krawczyk et al. 2018). In addition, LAES has an advantage over CAES and PHS due to not being constrained to geographical features (McLarnon and Cairns 1989). Although, micro-CAES systems are not constrained to geographic features and are effective in distributed

power networks (Kim et al. 2012, Kim and Favrat 2010). Highview Power Storage developed a 300kW LAES pilot plant in Slough, Scotland and have a 10MW commercial demonstration plant planned (Radcliffe and Williams 2013).

LAES has two main subsystems, air liquefaction subsystem and energy production subsystem. In the liquefaction subsystem, air is compressed, cooled, and expanded which produces liquid air. Multiple configurations like Linde-Hampson cycle, Claude cycle, Heylandt cycle, Collins cycle, and more, liquefy and store air (Barron 1985). The energy production system has multiple configurations like direct expansion method, indirect Rankine cycle, indirect Brayton multiple configurations like direct expansion method, indirect Rankine cycle, indirect Brayton cycle, and other variations that may be implemented (Lim, Al-Atabi, and Williams 2016). Storage is commonly included as a third subsystem, although this paper includes liquid air storage in the liquefaction subsystem.

There are multiple thermodynamic studies on liquid air energy storage available in literature. Early research in 1977 compressed air to 7 atm, dehumidified air and compressed further to 49 atm and cooled for storage; then re-pressurized liquid air to 80 atm before expanding through a turbine, which gave a efficiency up to 72% (Smith 1977). Guizzi et al. (2015) conducted a thermodynamic analysis of a LAES system with a multi-stage compressor and turbine, and a storage subsystem, which resulted in a round-trip efficiency of 54–55%. A similar system and analysis conducted by Kawczyk et al. (2016) showed round trip efficiencies from 45–57% when adjusting the inlet pressure to a JT valve. Another analysis demonstrated the effects on LAES energy efficiency when adjusting the compressor efficiency, compressor discharge pressure, and cryogenic pump discharge pressure (Xue et al. 2015). Additional work has focused on the liquefaction subsystem. Abdo et al. (2015) conducted a thermodynamic analysis on the Linde-Hampson cycle, Claude cycle, and Collins cycle and showed Claude and Collins cycles both having higher overall efficiencies than the Linde-Hampson cycle. Yu, Tian, and Xu (2009) conducted an exergy analysis of a Linde-Hampson cycle with an ejector and showed the addition of the ejector reduced the total exergy destruction in the cycle.

This paper presents an energy and exergy analysis of an ideal liquid air energy storage system. Energy is conserved through all processes and systems, but this is untrue for exergy (Moran and Shapiro 2004). Unlike exergy analysis, energy analysis does not account for the quality of energy; this makes exergy analysis useful when searching for areas of improvement within a system (Rosen and Dincer 2001, Lior and Zhang 2007). The analysis in this paper explores the upper bounds of energy efficiency and exergetic efficiency of the LAES system to identify optimal operating parameters.

C. SYSTEM DESCRIPTION

The liquid air energy storage system analyzed in this paper investigates the two different liquefaction subsystems, the simple Linde-Hampson cycle and the pre-cooled Linde-Hampson cycle; and two different energy production subsystems, a direct expansion method and the direct expansion method with additional heat added. Figure 15 displays the complete LAES system with alternative options to use either type of liquefaction subsystem or energy production subsystem.

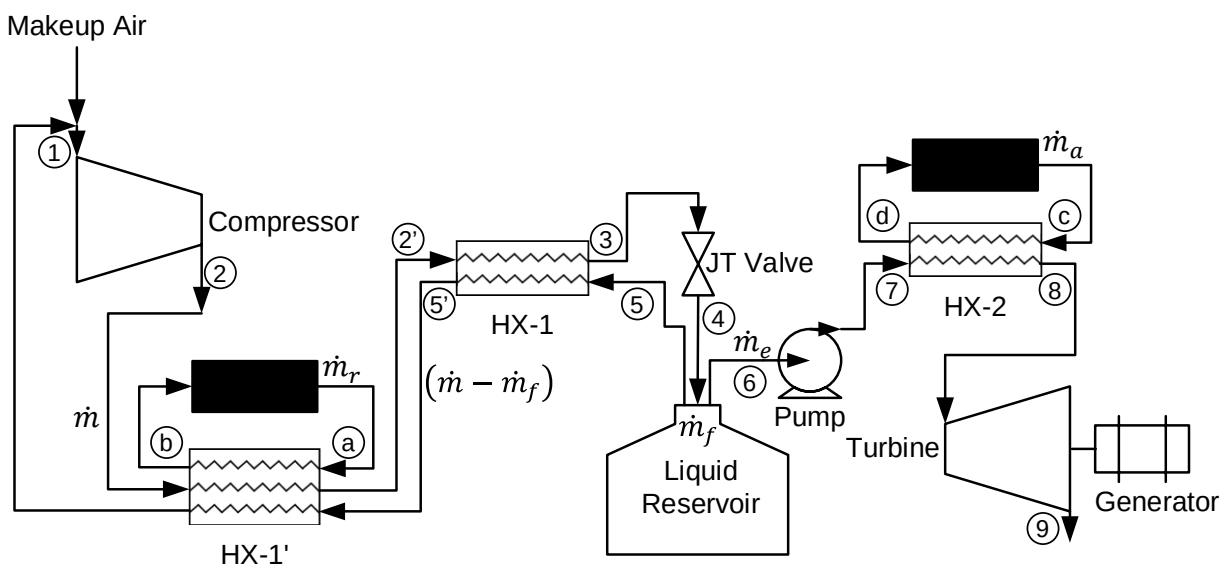

Figure 15. System Diagram of a Liquid Air Energy Storage System.

The simple Linde-Hampson cycle consists of a compressor, heat exchanger (HX-1), Joule-Thomson (JT) valve, and liquid reservoir. At steady state, mixing of makeup air and return air occurs prior to entering the compressor at state 1. Air is compressed to state 2 and then cooled in HX-1 to state 3. The cooled high-pressure air is expanded through the JT valve to state 4 where it is a two-phase mixture. The liquid reservoir stores liquid air at state 6 for later use by the energy production subsystem and the gas returns to HX-1 at state 5 providing the cooling from states 2 to 3. The pre-cooled Linde-Hampson system adds an additional heat exchanger, HX-1'. The subsystem providing the additional cooling in HX-1' is treated as a black box and only the required Q_{out} is calculated to achieve a desired state 2' temperature.

The direct expansion method for the energy production subsystem consists of a cryogenic pump, heat exchanger (HX-2), and turbine with a generator. The cryogenic pump pumps liquid air from the liquid reservoir to a desired pressure to state 7. Heat exchanger 2 heats pressurized liquid air to ambient temperature by the surrounding heat or available waste heat to state 8. A turbine then expands the evaporated air to generate electricity to state 9. The direct expansion method is a simple but an inefficient method to extract liquid air (Lim, Al-Atabi, and Williams 2016). The system can extract additional energy from the liquid air when heated beyond ambient temperature prior to entering the turbine. The Q_{in} represents the additional heat required to heat the liquid air above ambient pressure. Similar to HX-1', this is treated as a black box where the subsystem to achieve the required Q_{in} to reach a desired state 8 temperature is not considered.

Multiple combinations of state 2 pressures, state 2' temperatures, state 7 pressures, and state 8 temperatures can be used in this LAES system. Figure 16 shows an example of the system dynamics of the LAES system with one possible combination. The figure shows the liquefaction subsystem as states 1 through 5' where ambient air it pressurizes air to 20 MPa, precools to 250 K, and expands to generate approximately 21.3% liquid yield. The remaining gas passes through both heat exchangers, cooling the incoming air. States 6 through 9 represent the energy production subsystem. The subsystem pumps liquid air to 100 MPa, heats beyond ambient temperature to 350 K, and expands isothermally to state 9. This figure displays an ideal case for the LAES system where there is isothermal

compression and expansion, 100% effective heat exchangers, and an isentropic cryogenic pump.

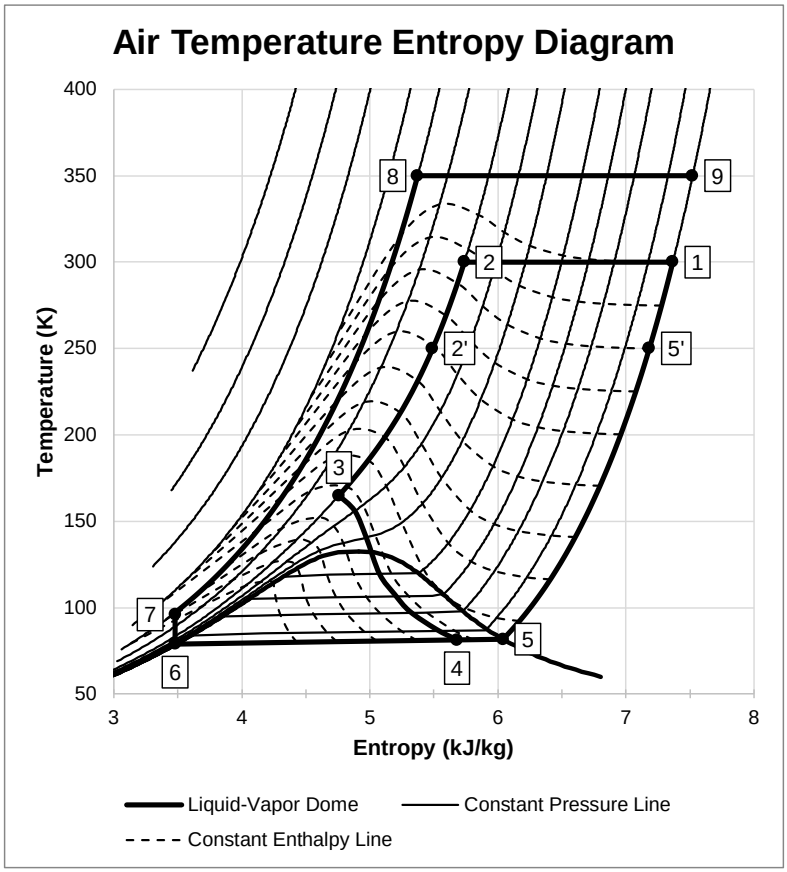

Figure 16. Air Temperature Entropy Diagram Showing Each State in the LAES System.

D. SYSTEM ENERGY ANALYSIS

As previously stated, this paper is investigating the upper bounds of an ideal LAES system. Therefore, all components are ideal components, the compressor isothermally compresses fluid, pumps isentropically compress fluids, heat exchangers are 100% effective, the turbine isothermally expands fluid, and there are no losses in lines. This section and the following section are organized by looking at each subsystem individually and then as a complete system.

1. Liquefaction Subsystem

The key information needed for the liquefaction subsystem is the required work for the compressor, the liquid yield, and required heat rejection from HX-1'. Using the first and second law on the compressor, the work per unit mass required to compress air from state 1 to 2 is (Barron 1985, Moran and Shapiro 2004, Kanoglu, Dincer, and Rosen 2008)

$$\frac{\dot{W}_c}{\dot{m}} = T_1(s_2 - s_1) + (h_1 - h_2). \tag{46}$$

This analysis calculated the liquid yield for the simple Linde-Hampson subsystem using a control volume encompassing HX-1, the JT valve, and liquid reservoir. The control volume excludes HX-1' and therefore, state 2 equals state 2' and state 5' equals state 1. Since there is no work or heat transferred to or from this control volume, the energy balance is (Barron 1985, Kanoglu, Dincer, and Rosen 2008)

$$\dot{m}h_2 = \dot{m}_f h_f + \left(\dot{m} - \dot{m}_f\right)h_1 . \tag{47}$$

The ratio of liquid mass flow rate to mass flow rate provides the liquid yield for the simple Linde-Hampson subsystem

$$Y = \frac{\dot{m}_f}{\dot{m}} = \frac{h_2 - h_1}{h_f - h_1} . \tag{48}$$

The compressor work per unit mass liquefied is therefore the compressor work per unit mass divided by the liquid yield.

$$\frac{\dot{W}_c}{\dot{m}_f} = \frac{\dot{W}_C}{\dot{m}Y} = [T_1(s_2 - s_1) + (h_1 - h_2)]\left(\frac{h_f - h_1}{h_2 - h_1}\right) \tag{49}$$

The pre-cooled Linde-Hampson system requires the use of a second heat exchanger (HX-1') (Barron 1985). There are two cooling streams, $\dot{Q}_{out}$ stream and the returning air stream. The required $\dot{Q}_{out}$ for any desired temperature at state 2' is based on the energy balance of HX-1' (Barron 1985).

$$\dot{m}_r h_a + \dot{m} h_2 + \left(\dot{m} - \dot{m}_f\right) h_{5'} = \dot{m}_r h_b + \dot{m} h_{2'} + \left(\dot{m} - \dot{m}_f\right) h_1 \qquad (50)$$

Assuming the mass flow rate through the liquefaction subsystem, $\dot{m}$, is equal to the mass flow rate in the black box subsystem, $\dot{m}_r$, rearranging the equation and solving for Q_{out} per unit mass gives

$$\frac{\dot{Q}_{out}}{\dot{m}} = h_a - h_b = (h_{2'} - h_2) + (1 - Y)(h_1 - h_{5'}) \,. \qquad (51)$$

Using the previous control volume but now including HX-1', the energy balance is (Barron 1985)

$$\dot{m}_r h_a + \dot{m} h_2 = \dot{m}_r h_b + \left(\dot{m} - \dot{m}_f\right) h_1 + \dot{m}_f h_6 \,. \qquad (52)$$

Defining the black box subsystem mass flow-rate ratio as (Barron 1985)

$$r = \frac{\dot{m}_r}{\dot{m}} \,, \qquad (53)$$

the yield of the pre-cooled Linde-Hampson subsystem is therefore

$$Y = \frac{\dot{m}_f}{\dot{m}} = \frac{h_2 - h_1}{h_f - h_1} + r\frac{h_a - h_b}{h_f - h_1} \,. \qquad (54)$$

As Equation (54) shows, pre-cooling provides additional liquid yield. This analysis uses the assumption that the ratio, *r*, is equal to one and 100% effective heat exchangers. Therefore, the liquid yield of the subsystem is unchanged from Equation (48).

2. Energy Production Subsystem

The energy calculations needed for the direct expansion method is the cryogenic pump work and the turbine work. The analysis assumes that the mass flow rate of the energy production subsystem is equal to the mass flow rate of the liquefaction subsystem. Additionally, the analysis assumes the pump isentropically compresses liquid air and there are no heat losses in the pump. Using these assumptions, the pump work is defined as

$$\frac{\dot{W}_p}{\dot{m}} = h_6 - h_7, \tag{55}$$

assuming isothermal expansion, the turbine work is

$$\frac{\dot{W}_t}{\dot{m}} = T_8(s_9 - s_8) + (h_8 - h_9). \tag{56}$$

No work is associated with HX-2 for the direct expansion method. This ideal system assumes the compressed liquid air reaches ambient temperature through a heat exchanger by means of the surrounding air or by waste heat recovery. Although this is not practical in a real system, this is a step in ensuring the analysis determines the true upper bounds of the system. Providing additional heat to HX-2 allows state 8 to reach temperatures beyond ambient temperature. The analysis assumes additional heat required is only heat required beyond 300 K at a particular pressure. Therefore, assuming the mass flow rate of the heating source is equivalent to the mass flow rate of the energy production subsystem, the equation for additional heat is

$$\frac{\dot{Q}_{in}}{\dot{m}} = h_8 - h_{300K}, \tag{57}$$

where h_{300K} is the enthalpy of air at a temperature of 300 K at a given pressure.

3. Complete LAES System

The first law measure of performance for the complete LAES system is the overall system efficiency, or round trip efficiency. The equation to calculate the overall system efficiency is dependent on the subsystems used. The simple Linde-Hampson subsystem with direct expansion method has work inputs to the compressor and pump from equations (49) and (55), respectively. The heat rejection required from $\dot{Q}_{out}$ in HX-1' for the pre-cooling Linde-Hampson subsystem requires additional work to be performed. This work is calculated as the work required for a Carnot refrigerator (Moran and Shapiro 2004)

$$\frac{\dot{W}_{HX_{1'}}}{\dot{m}_f} = \frac{\dot{Q}_{out}}{\dot{m}_f}\left(\frac{T_1}{T_{5'}} - 1\right). \tag{58}$$

Given liquid air is the working fluid, using work per unit mass liquefied is preferred for energy efficiency calculations. When the temperature of state 8 exceeds ambient temperatures, additional work is required to add the necessary heat to achieve this temperature. This additional work is defined as the work required for a Carnot heat pump (Moran and Shapiro 2004).

$$\frac{\dot{W}_{HX_2}}{\dot{m}_e} = \frac{\dot{Q}_{in}}{\dot{m}_e}\left(1 - \frac{T_7}{T_8}\right) \tag{59}$$

The overall system efficiency is the ratio of work output to inputs.

$$\eta_{sys} = \frac{\dot{W}_t}{\left(\dot{W}_C/_Y\right) + \dot{W}_p + \dot{W}_{HX_1'} + \dot{W}_{HX_2}} \tag{60}$$

E. SYSTEM EXERGY ANALYSIS

The below exergy analysis uses a steady-state exergy rate balance to calculate the exergy destruction within a given component, as seen in Equation (61) (Moran and Shapiro 2004)

$$0 = \sum\left(1 - \frac{T_0}{T_j}\right)\dot{Q}_j - \dot{W}_{cv} + \sum \dot{m}_i\psi_i - \sum \dot{m}_e\psi_e - \dot{I}, \tag{61}$$

where the exergy flow, ψ, is defined as (Moran and Shapiro 2004),

$$\psi_i = h_i - h_0 - T_0(s_i - s_0) + \frac{V_i^2}{2} + gz_i\ . \tag{62}$$

This analysis assumes kinetic and potential energy terms are negligible, and therefore Equation (62) reduces to

$$\psi_i = h_i - h_0 - T_0(s_i - s_0)\ . \tag{63}$$

The dead state temperature, T_0, is assumed to be 300 K at a pressure of 0.101325 MPa. The analysis will present the calculations of the exergy destruction rate, $\dot{I}$, and exergetic efficiency, ε, for each component and the system.

1. Liquefaction Subsystem

From state 1 to 2, there is no temperature change, and therefore, the compressor exergy destruction rate is

$$\dot{I}_c/\dot{m} = -\dot{W}_c/\dot{m} + \psi_1 - \psi_2 \,. \tag{64}$$

Substituting in Equation (63)

$$\dot{I}_c/\dot{m} = -\dot{W}_{cv}/\dot{m} + h_1 - h_2 - T_0(s_1 - s_2), \tag{65}$$

the exergetic efficiency for the compressor is (Moran and Shapiro 2004, Kanoglu 2002),

$$\varepsilon_c = \psi_2 - \psi_1 \Big/ \left(-\dot{W}_{cv}/\dot{m}\right) \,. \tag{66}$$

Assuming the mass flow rates $\dot{m} = \dot{m}_r$ with no work or heat loss, the exergy destruction rate for HX-1' is (Paniagua et al. 2013)

$$\dot{I}_{HX_{1'}}/\dot{m} = (\psi_2 - \psi_{2'}) + (\psi_a - \psi_b) + (1 - Y)(\psi_{5'} - \psi_1). \tag{67}$$

The exergetic efficiency for HX-1' is the ratio of the exergy increase of the hot stream to the exergy decrease in the cold streams (Moran and Shapiro 2004, Kanoglu 2002).

$$\varepsilon_{HX_{1'}} = (\psi_2 - \psi_{2'}) \Big/ (\psi_b - \psi_a) + (1 - Y)(\psi_1 - \psi_{5'}) \tag{68}$$

The exergy destruction and exergetic efficiency for HX-1 is

$$\dot{I}_{HX_1}/\dot{m} = (\psi_{2'} - \psi_3) + (1 - Y)(\psi_5 - \psi_{5'}) \tag{69}$$

$$\varepsilon_{HX_1} = (\psi_{2'} - \psi_3)/(1 - Y)(\psi_{5'} - \psi_5) \quad . \tag{70}$$

The analysis assumes there is no work or heat transfer to the surroundings for fluid flow through the JT valve. In addition, there is no change in enthalpy during a throttling process; therefore, the exergy destruction rate reduces to

$$\dot{I}_{JT}/\dot{m} = T_0(s_4 - s_3)\,. \tag{71}$$

The JT valve exergetic efficiency is defined as the ratio of the exergy flow out to the exergy flow in (Kanoglu 2002).

$$\varepsilon_{JT} = \psi_4/\psi_3 \tag{72}$$

The analysis completes the calculation for the simple Linde-Hampson subsystem exergetic efficiency by taking the ratio of the reversible work to the actual work (Kanoglu, Dincer, and Rosen 2008, Borri et al. 2017). The reversible work is the difference in exergy flow of states 1 and 6 (Kanoglu, Dincer, and Rosen 2008).

$$w_{rev} = \psi_6 - \psi_1 = h_6 - h_1 - T_0(s_6 - s_1) \tag{73}$$

The simple Linde-Hampson subsystem exergy efficiency is

$$\varepsilon_{sLH} = w_{rev}/\left(\dot{W}_C/Y\right)\,. \tag{74}$$

The pre-cooled Linde-Hampson subsystem exergy efficiency must also account for the from work input to HX-1'.

$$\varepsilon_{pcLH} = w_{rev}/\left(\dot{W}_C/Y + \dot{W}_{HX_{1'}}\right) \tag{75}$$

2. Energy Production Subsystem

The ideal pump is assumed to be isentropic, which results in an exergy destruction rate of

$$\dot{I}_p / \dot{m}_e = -\dot{W}_p / \dot{m}_e + h_6 - h_7. \tag{76}$$

The exergetic efficiency of the pump is

$$\varepsilon_p = \psi_7 - \psi_6 \Big/ \left(-\dot{W}_p / \dot{m}_e \right). \tag{77}$$

Assuming the mass flow rates $\dot{m}_a$ and $\dot{m}_e$ are equivalent, the exergy destruction and exergetic efficiency of HX-2 is

$$\dot{I}_t / \dot{m}_e = (\psi_c - \psi_d) + (\psi_7 - \psi_8) \tag{78}$$

$$\varepsilon_{HX_2} = (\psi_7 - \psi_8) \big/ (\psi_d - \psi_c). \tag{79}$$

The ideal turbine is assumed to be isothermal, which results in an exergy destruction rate of

$$\dot{I}_t / \dot{m}_e = -\dot{W}_t / \dot{m}_e + \psi_8 - \psi_9 \,. \tag{80}$$

The exergetic efficiency of the turbine is

$$\varepsilon_t = \psi_9 - \psi_8 \Big/ \left(-\dot{W}_t / \dot{m}_e \right). \tag{81}$$

3. Complete LAES System

The total exergy destruction rate of the system is the sum of all component exergy destruction rates from equations (64), (67), (69), (71), (76), (78), and (80). The exergetic efficiency for the entire LAES system is defined as (Kanoglu 2002)

$$\varepsilon_{sys} = {\dot{W}_{act} - \dot{I}_{tot}}/{\dot{W}_{act}}, \tag{82}$$

where $\dot{W}_{act}$ is the sum of all work inputs

$$\dot{W}_{act} = \dot{W}_C + \dot{W}_p + \dot{W}_{HX_1'} + \dot{W}_{HX_2}. \tag{83}$$

F. RESULTS AND DISCUSSION

1. First Law Results and Discussion

The following results use values of enthalpy and entropy gathered from (Lemmon et al. 2000). The tables available from Lemmon et al. (2000) provide only discrete iso-pressure values as shown in Table 4.

Table 4. List of Iso-Pressures Available from Lemmon et al.

Pressure (MPa)	0.101325	0.2	0.5	1	2	5	10
	20	50	100	200	500	1000	2000

The analysis found that the pressure range for the liquefaction subsystem to produce any liquid yield is 5 MPa to 100 MPa; at 200 MPa, the liquid yield drops to zero. Figure 17 shows the liquid yield for the simple Linde-Hampson subsystem. These results match results found in (Barron 1985, Joshi and Patel 2015). The maximum yield point found by Joshi and Patel was 0.107 at a pressure of 32 MPa, which is represented on Figure 17 with an “x.”

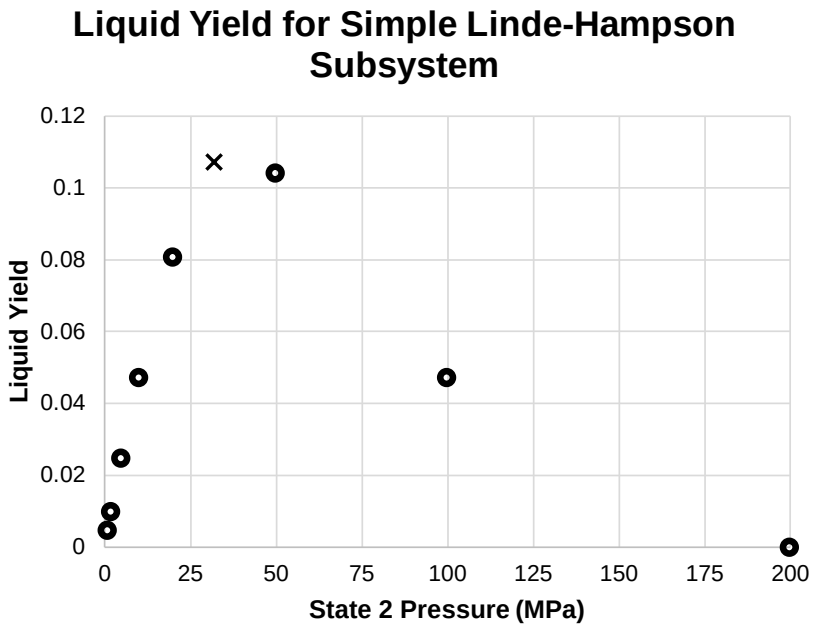

Figure 17. Liquid Yield for Simple Linde-Hampson Subsystem over Varying State 2 Pressures.

Figure 18 shows an alternative view of the liquid yield for the simple Linde-Hampson subsystem. The expansion of air from state 3 to 4 is an isenthalpic process. This throttling process must follow the lines of constant enthalpy shown on a temperature entropy diagram. Figure 18 shows the lines of constant enthalpy followed over the different state 2 pressures. This figure also shows the corresponding state 3 temperature for each state 2 pressure. The state 3 temperature is important when considering the required effectiveness of a heat exchanger to reach this temperature.

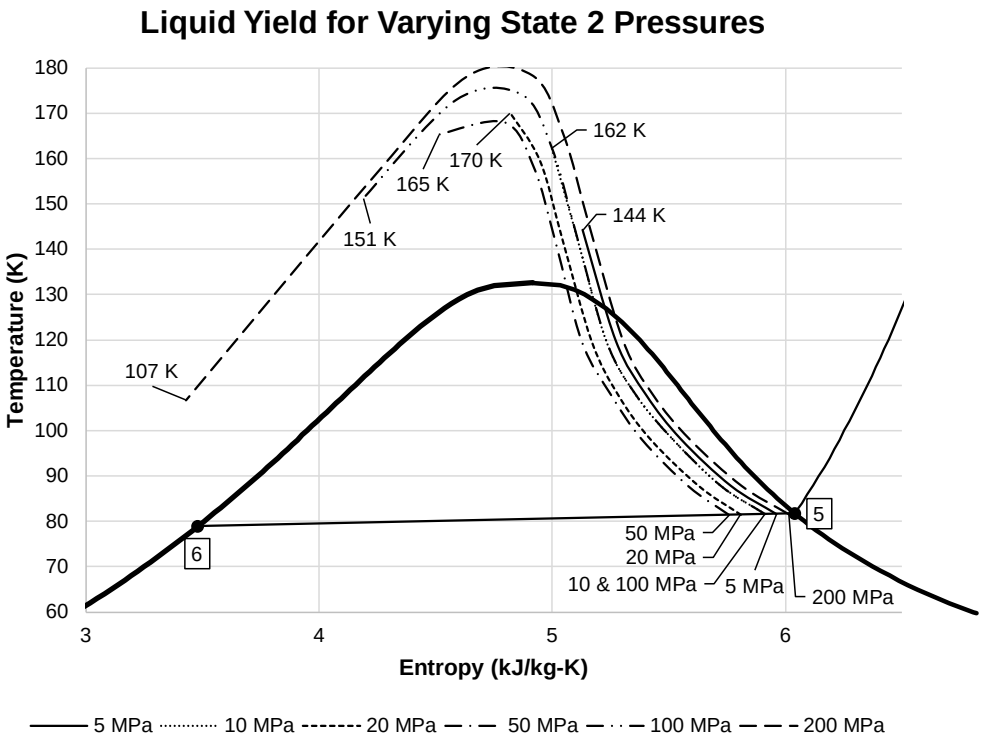

Figure 18. Air Temperature Entropy Diagram Showing Liquid Yield with Lines of Constant Enthalpy from State 3 to State 4.

Displayed in Figure 19, the resulting compressor work per unit mass liquefied shows the optimal state 2 pressure is around 20 to 50 MPa. The liquid yield of this system is likely to be a key measure of performance for a building-scale LAES system. Quickly replenishing liquid air supply ensures continued support during peak demands. Figure 20 shows the liquid yield for the pre-cooled Linde-Hampson subsystem. This figure clearly shows the improvement of liquid yield over all pressures with pressures of 20 and 50 MPa producing the highest liquid yield.

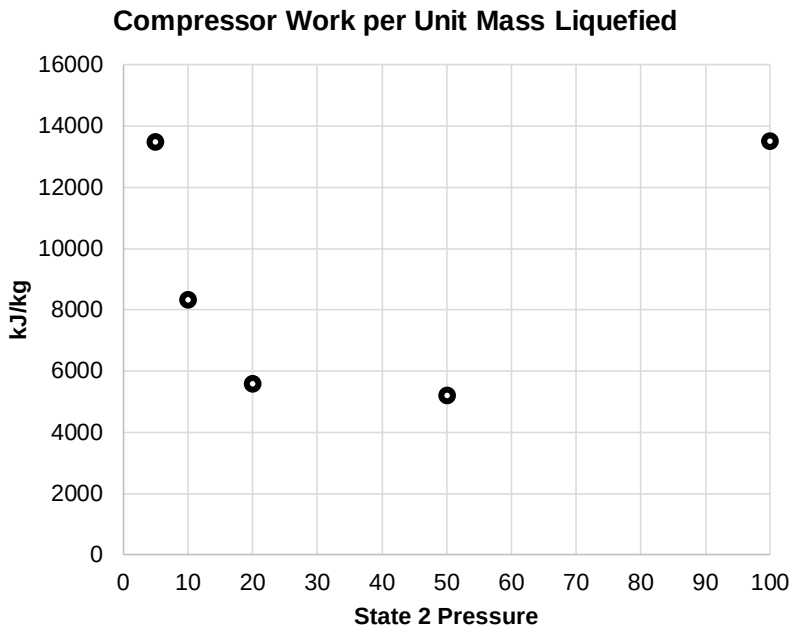

Figure 19. Compressor Work per Unit Mass Liquefied for Simple Linde-Hampson Subsystem.

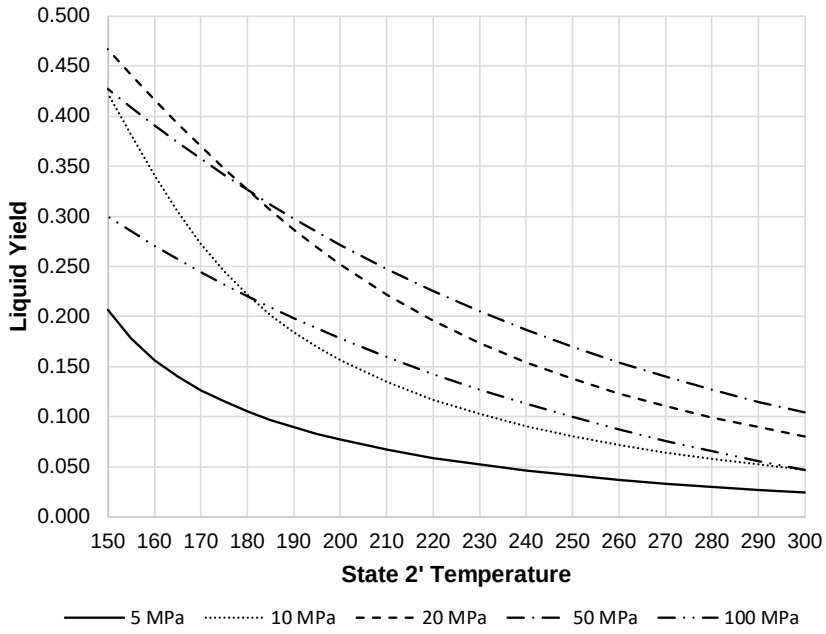

Figure 20. Liquid Yield for Pre-cooled Linde-Hampson Subsystem with Varying State 2 Pressures.

When the liquid increases, this reduces the work required by the compressor on a per unit mass liquefied basis. Figure 21 shows the resulting compressor work per unit mass liquefied for the pre-cooled Linde-Hampson subsystem. This figure shows all pressures begin to converge, except 100 MPa, at a state 2' temperature around 250 K.

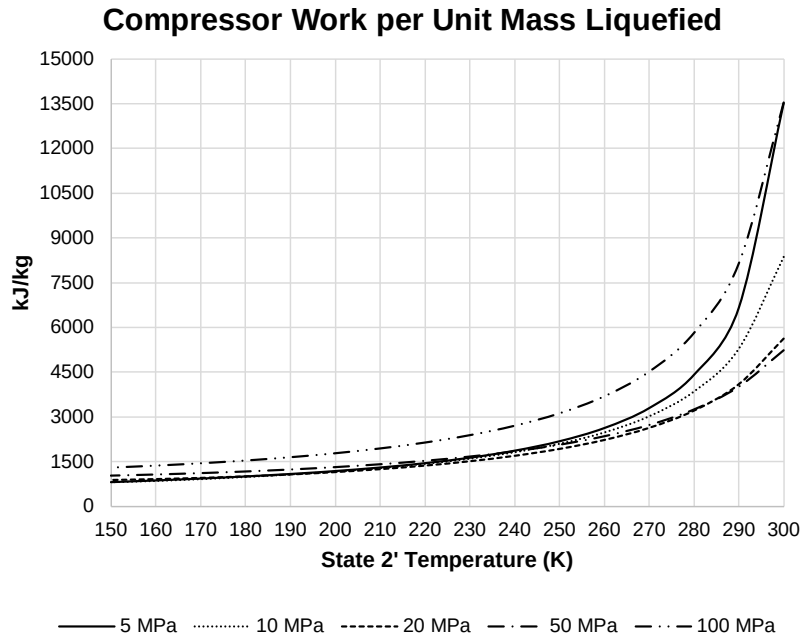

Figure 21. Compressor Work for Pre-cooled Linde Subsystem with Varying State 2 Pressures.

In order to achieve a desired state 2' temperature, the system must remove additional heat from the pressurized air stream in HX-1'. Figure 22 displays the additional heat removed from this stream by the external black box system. As the required heat removal increases, required total work of the liquefaction subsystem increases. Figure 23 presents the total work required by the pre-cooled liquefaction subsystem. This figure shows the same convergence of pressures as Figure 21, but also displays the impact HX-1'. The required work at temperatures below 220 K begins to level out and then begins to increase at approximately 150 K.

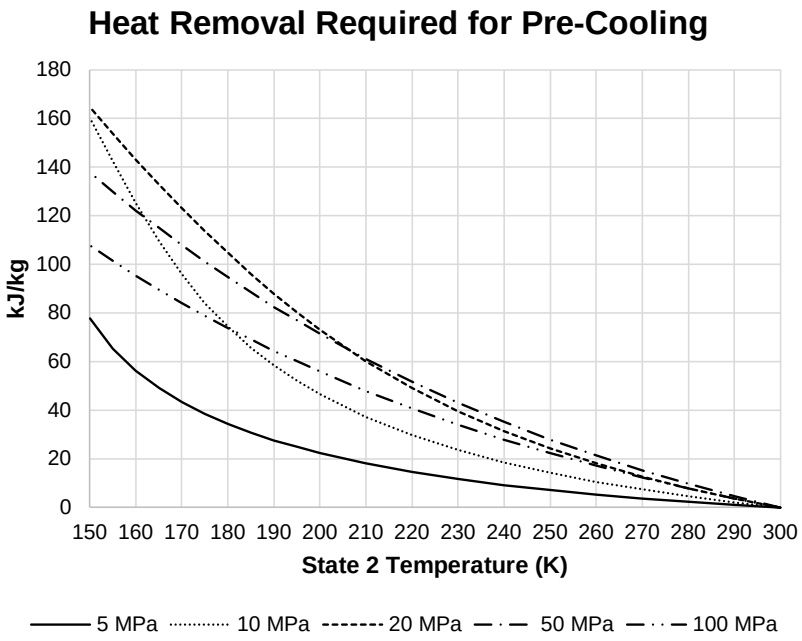

Figure 22. Required Heat Removal for Pre-cooled Linde-Hampson Subsystem.

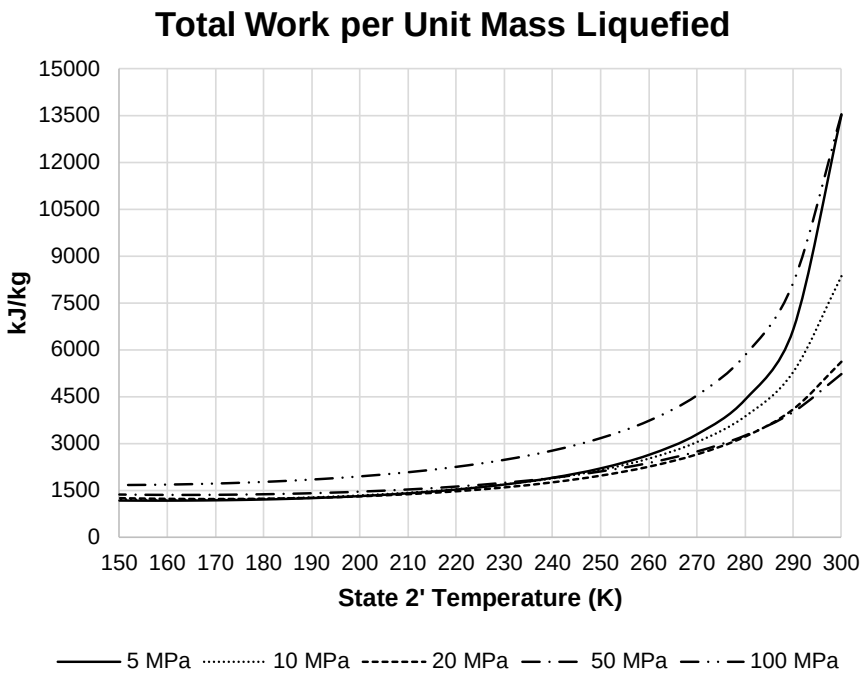

Figure 23. Total Work per Unit Mass Liquefied for the Pre-cooled Liquefaction Subsystem.

The LAES system efficiency is dependent on multiple factors, including state 2 pressure, state 2' temperature, state 7 pressure, and state 8 temperature. Figure 24 displays the resulting LAES system energy efficiency when using state 2 and 7 pressures and state 2' temperature as chosen factors. There is a clear increase of system efficiency as the state 2' temperature is reduced and state 7 pressure is increased. Similar to the compressor work per unit mass liquefied results in Figure 21, the LAES system efficiency peaks at state 2 pressures around 20 and 50 MPa.

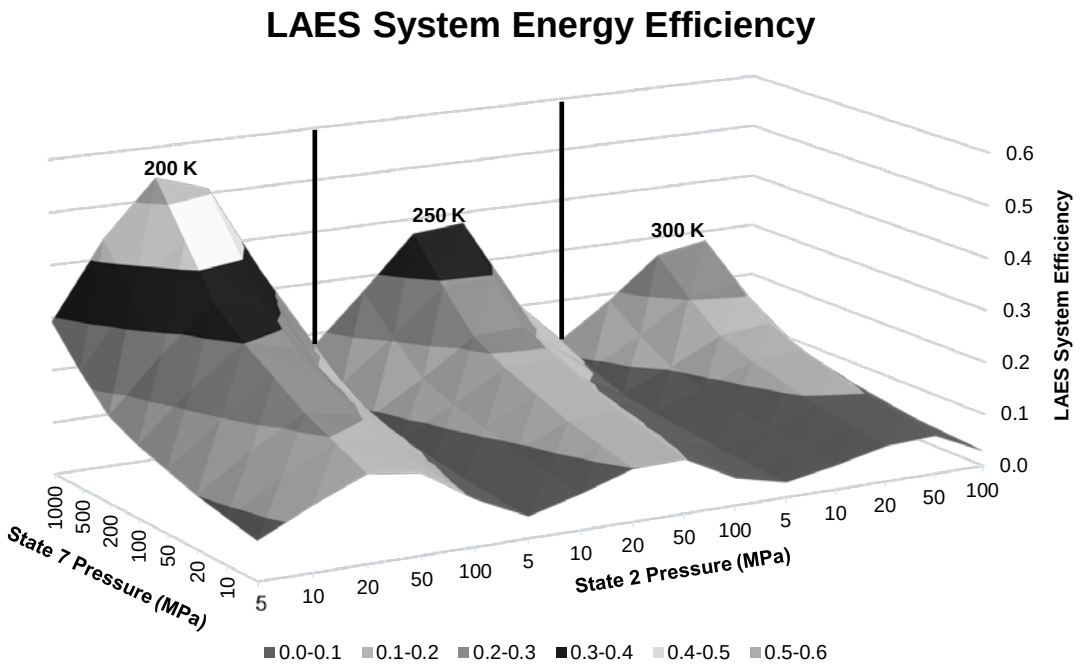

Figure 24. Resulting LAES System Energy Efficiency with Varying State 2 and 7 Pressures and Three State 2' Temperatures.

Figure 25 presents a narrower view of Figure 24 by reducing to only three state 2 pressures of 10, 20, and 100 MPa. This figure depicts a clear gain in energy efficiency choosing 20 MPa and lower state 2' temperatures. Although, the ranges presented on the figure may not be achievable in a building-scale LAES system. Maximum state 7 pressure is likely to be approximately 100 MPa given size restrictions for a building-scale system. A state 2' temperature of 250K is likely to be attainable. At these factors, the approximate

LAES system efficiency at 20 MPa is 18.4%. Increasing the temperature into the turbine inlet increases the energy efficiency of the LAES system. Figure 26 depicts this increase in energy efficiency using a state 2' temperature of 250 K and state 7 pressure of 100 MPa.

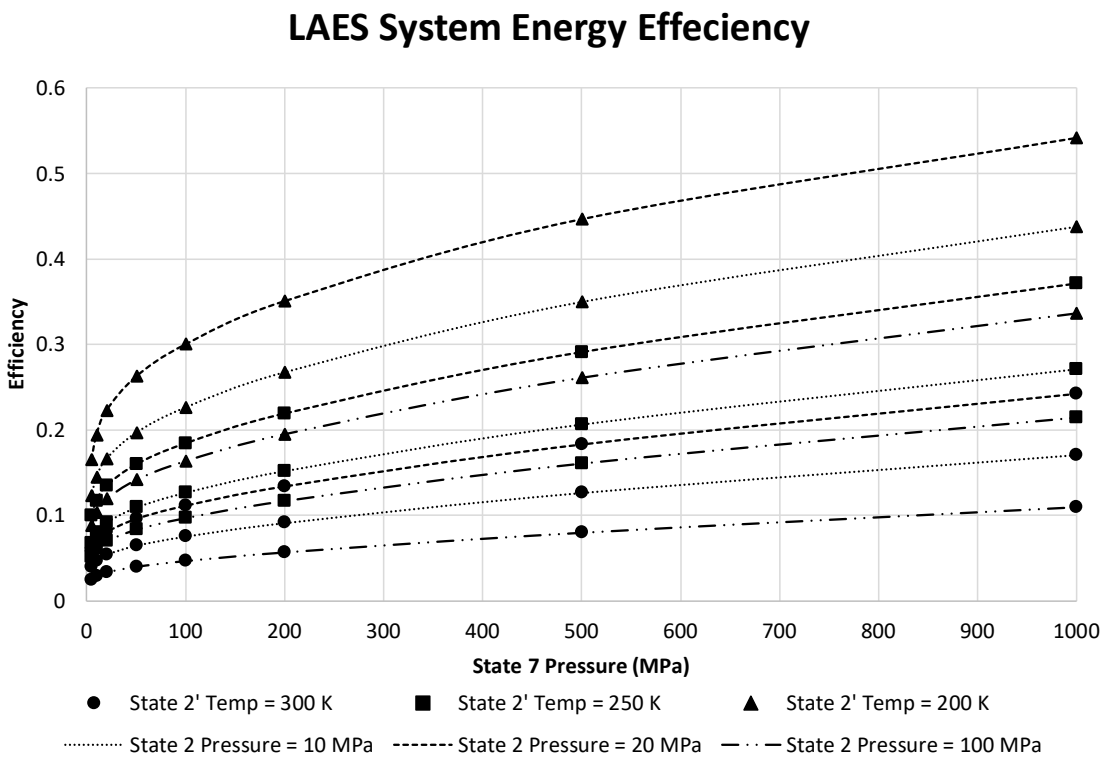

Figure 25. Resulting LAES System Energy Efficiency over Full Range State 7 Pressures and three Selected State 2' Temperatures and State 2 Pressures.

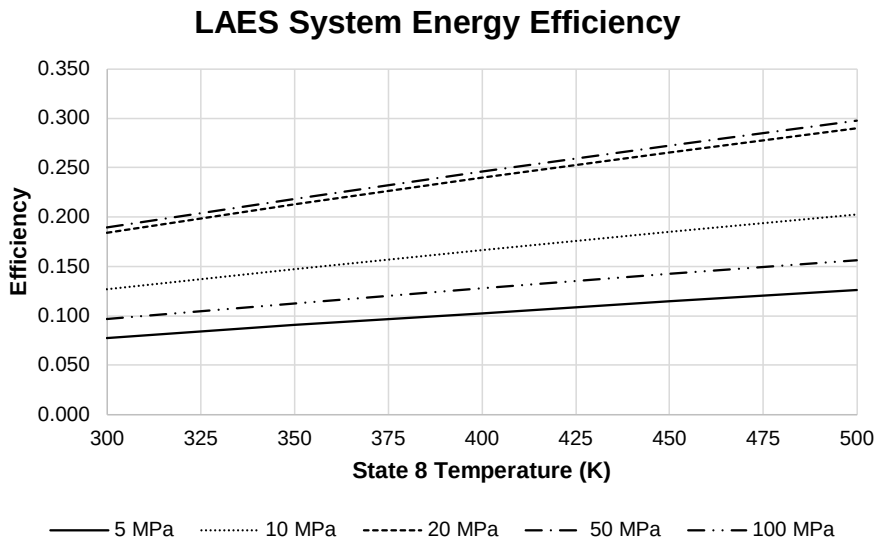

Figure 26. Effects of Increasing State 8 Temperature on LAES Energy Efficiency at a State 2' Temperature of 250K and State 7 Pressure of 100 MPa.

2. Second Law Results and Discussion

The exergy destruction and exergetic efficiency of the compressor, HX-1', the pump, HX-2, and the turbine are trivial due to using ideal cases. The exergy destruction for each of these components are zero and the exergetic efficiency is equal to one. Although this is not the case for the turbine when the temperature at state 8 exceeds 300 K. The largest attributer to exergy destruction in this system is the JT valve. Figure 27 shows the JT valve exergetic efficiency over different state 2 pressures when decreasing the state 2' temperature. The optimal state 2 pressure in terms of exergetic efficiency for the JT valve is 20 MPa.

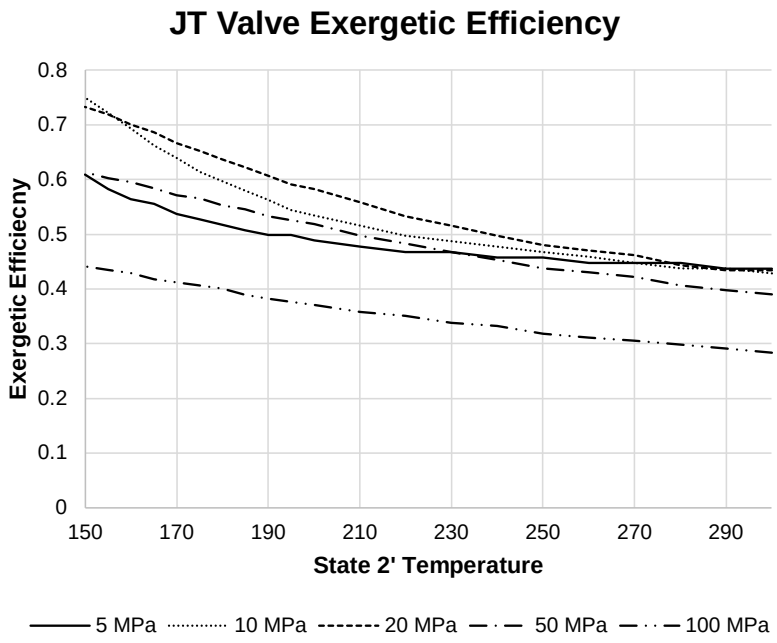

Figure 27. JT Valve Exergetic Efficiency with Varying State 2 Pressures and State 2' Temperatures.

Figure 28 displays the exergetic efficiency of HX-1 over varying state 2' temperatures and state 2 pressures. This component shows 20 MPa as the worst pressure in terms of exergetic efficiency. Although at this pressure, the exergy destruction rate of HX-1 is substantially less than the JT valve, and therefore, has less impact on the overall system exergetic efficiency. Figure 29 depicts these two components exergy destructions at a state 2 pressure of 20 MPa.

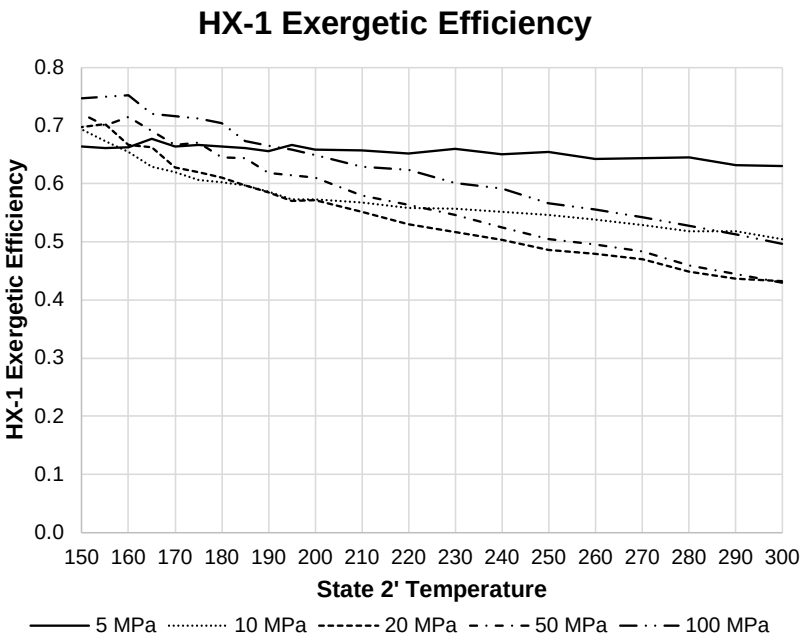

Figure 28. HX-1 Exergetic Efficiency with Varying State 2 Pressures and State 2' Temperatures.

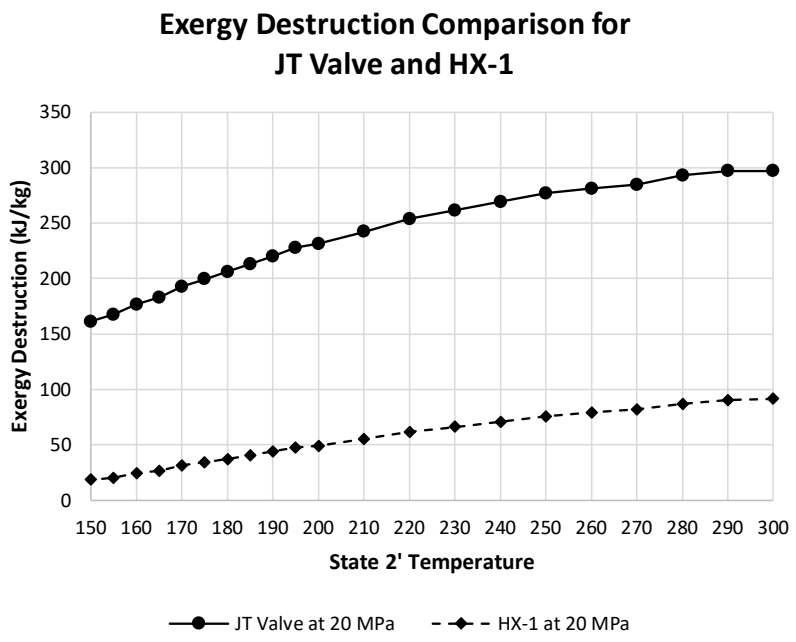

Figure 29. Exergy Destruction Comparison of the JT Valve and HX-1 at a State 2 Pressure of 20 MPa over varying State 2' Temperatures.

Figure 30 shows the exergetic efficiency of the liquefaction subsystem. This figure again shows that 20 MPa to 50 MPa are an optimum pressure range. Figure 31 displays the changes in the LAES system exergetic efficiency when changing the state 2' temperature and pressure. The optimum pressure displayed on the figure is 20 MPa.

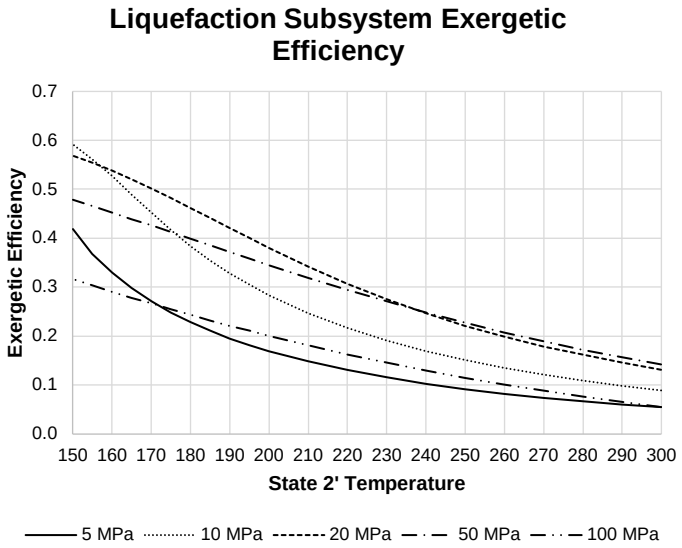

Figure 30. Exergetic Efficiency of the Liquefaction Subsystem.

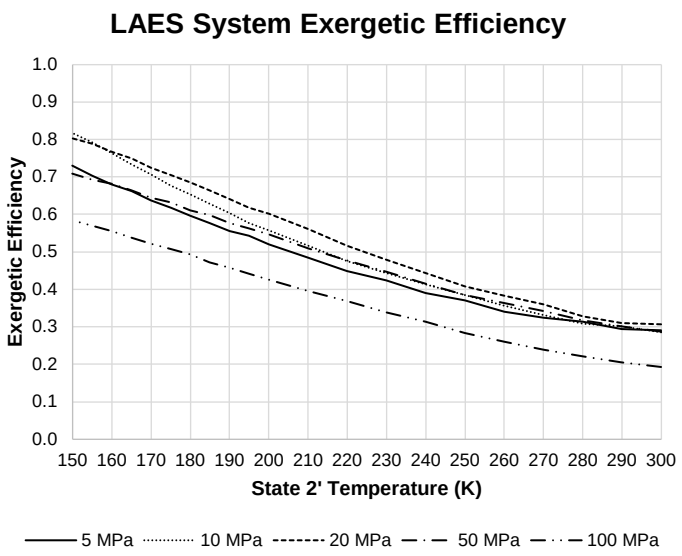

Figure 31. LAES System Exergetic Efficiency at a State 7 Pressure of 100 MPa and State 8 Temperature of 300 K.

G. CONCLUSION

This paper conducted an energy and exergy analysis of an ideal liquid air energy storage system. The results showed that the pre-cooled Linde-Hampson subsystem was superior to the simple Linde-Hampson subsystem, and heating liquid air beyond ambient temperature was superior to heating to only ambient. The optimal state 2 pressure range was 20 to 50 MPa where there was maximum liquid yield. Pre-cooling resulted in an increase in liquid yield, energy efficiency, and exergetic efficiency. Although, pre-cooling below 150 K will result in increased total work per unit mass liquefied. Heating the liquid air beyond ambient temperature results in increased electrical generation and increases the overall efficiency of the system.

Additional improvement of the energy and exergetic efficiency may be found with alternative liquefaction subsystems, which utilize an expander, such as the Claude and Heylandt systems. The system would be improved further by incorporating cold and heat recovery systems, as used by previous work which achieved round trip efficiencies of 45-57%.

H. ACKNOWLEDGMENTS

This work was sponsored by ESTEP (Energy Systems Technology Evaluation Program) funded by the Office of Naval Research under the technical monitors of Richard Carlin and Marissa Brand.

V. NIST CADDIE

A. BACKGROUND AND INTRODUCTION

When performing any thermodynamic analysis, the user needs data tables or formulas to determine the needed fluid properties, such as the enthalpy and entropy, at any given temperature, pressure, or density. The National Institute of Standards and Technology maintains the NIST Chemistry WebBook, SRD 69, which provides thermophysical properties for 74 different fluids. A user selects a fluid, chooses the units desired, the type of data, the database, and the range of values to look up. A limitation of the webpage is that data tables are limited to approximately 600 data points. If a user selects a large range of data, the website will adjust the intervals to meet this 600 data point restriction, regardless of the interval selected. Depending on the range of data selected, this would cause a low resolution between data points. The user may choose a smaller range to have a more refined interval between data points, although, this may not cover the entire range desired. The user would then need to download multiple data tables to cover the complete range needed. An additional limitation is that the webpage provides the data in an html table or in a tab-delimited text file format only. If the user is utilizing Excel to conduct calculations, as this thesis did, transferring data tables to Excel becomes cumbersome and time consuming.

The NIST Caddie tool provides a solution to this problem. The tool utilizes Excel user forms to match the experience of the NIST website. The NIST Caddie is an Excel-add-in requiring a user simply to download a single file and install it. Users can seamlessly select from the same fluids, choose the same units, and reference data from the same data types. It can support any range of data that is allowable by the NIST website.

Figure 32 displays a general flowchart of the NIST Caddie. Once a user has selected the fluid parameters, the add-in first determines if the range of data selected exceeds 600 data points. If the data range is less than 600, then it is a single set and the program executes a single query from the NIST webpage. If the data range exceeds 600,

then the program determines the required number of sets, creates a primary worksheet, and loads a progress bar. A number of sets is the total number of data points divided by 600.

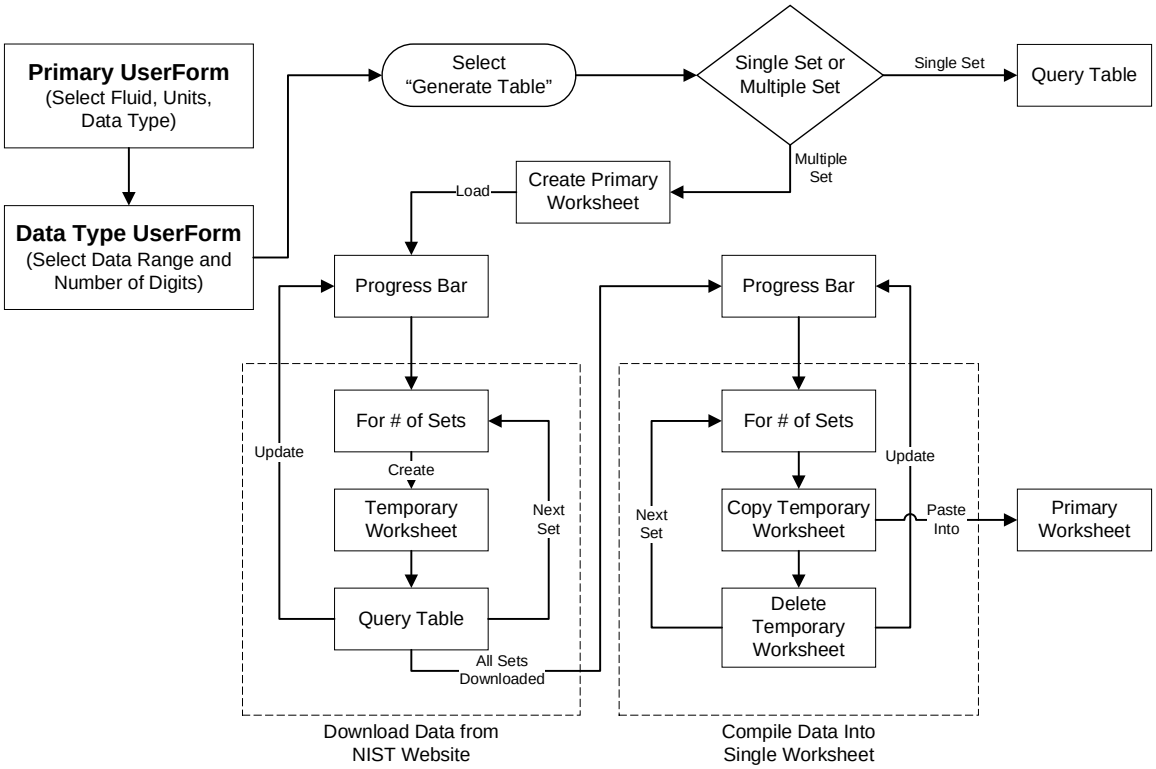

Figure 32. NIST Caddie Flowchart.

The program then enters the download loop based on the number of sets calculated. The program creates a temporary worksheet and then sends a query to the NIST website for the data range in the current set. The progress bar is updated and then the loop moves on to the next set. Once all sets have been downloaded, the program moves to the compile data loop. First, a new progress bar loads and then the compile data loop begins. The program copies each temporary worksheet, pastes it into the primary worksheet, and deletes the temporary worksheet. The final product of executing the program is a single worksheet with the complete range and interval of data requested.

This tool was vital in completing the Chapter III of this thesis. A researcher or educator cannot complete a fundamental thermodynamic analysis without valid and usable

tables. The National Institute of Standard and Technology utilizes the most recent research to create and compile their tables. Downloading these tables into an Excel worksheet makes the tables usable for easy calculations and generation of charts and figures. Researchers will find this tool useful when faced with limited resources or when conducting fundamental analyses to validate simulations. Educators will find this tool useful when teaching thermodynamic subjects and wish to have a visual representation of different cycles or the impact of changing different parameters in an analysis.

B. NIST CADDIE SETUP AND INSTRUCTIONS

Those interested in using the NIST Caddie should see the Supplemental section to locate a copy of the add-in. The setup instructions provided in this section assume the user is using Excel 2016. If a different version is in use, the author recommends going to the Microsoft help webpage to complete the setup. To add an Excel add-in, with an Excel worksheet open, go to File → Options. On the left hand side, select "Add-ins." At the bottom, under the drop down for "Manage," select "Excel Add-ins" and press the button "Go." Next select "Browse," locate and select the file location of the NIST Caddie add-in, and select "Ok."

In order to execute NIST Caddie, the user must add a button to the Excel ribbon. To add a button to the ribbon, go to File → Options. Next, select "Customize Ribbon" from the left hand side. The user will now see on the right hand side a list of all the ribbon options under the "Main Tabs." Next, expand the "Home" tab and create a new group button selection the button below name "New Group." The user will now see a new group created, highlight by selecting this new group. On the left under "Choose commands from:" select the option macros from the drop down bar. Next, scroll and find the macro named "NIST_Caddie," select this macro, and select the button in the center named "Add." At the bottom right select "Ok" and the new button will be located under the Home tab.

In order to generate a data table, select the new button in the ribbon named "NIST_Caddie." Figure 33 shows the primary Excel user form where the user will select the fluid, units, and data type.

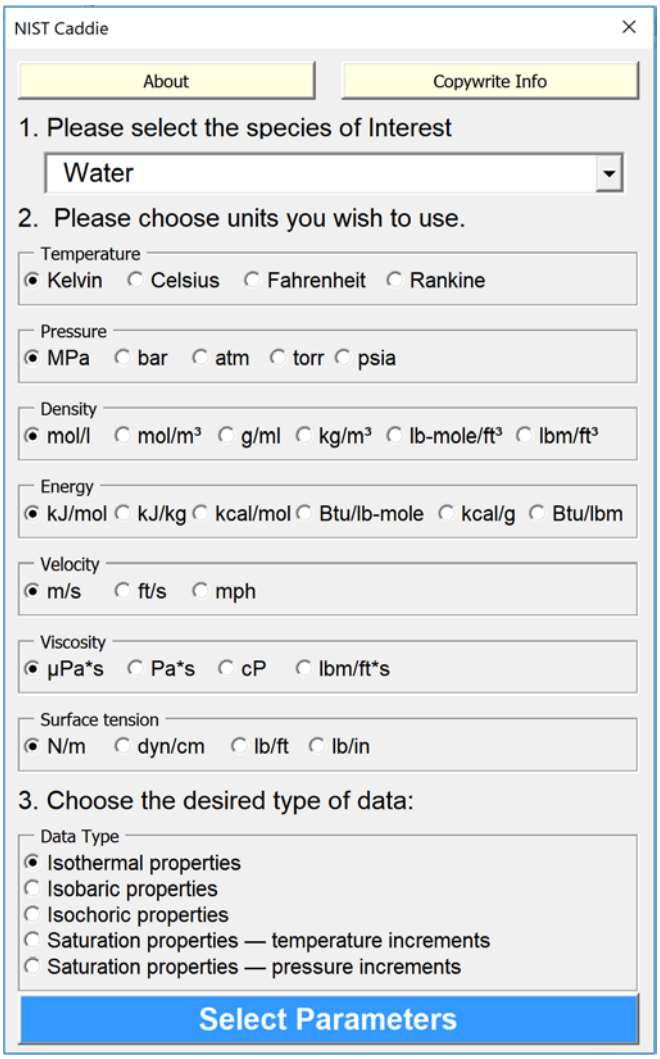

Figure 33. Image of the Primary Excel User Form in the NIST Caddie.

After selecting "Select Parameters," the next user form will appear based on the data type selected and allow the user to input the range of data needed. Figure 34 displays the options available if the user selected all options from Figure 33. This user form displays the data type and fluid chosen in the title bar, "Isothermal Properties for Water." This provides confirmation to the user that the program is referencing the correct fluid. The user must adhere to the allowable data ranges displayed on the user form. The number of digits option is the number of significant digits required by the user. Be warned, if a user requests a large data range at small intervals with the maximum number of digits, the file size for the data table will easily exceed 100 MB.

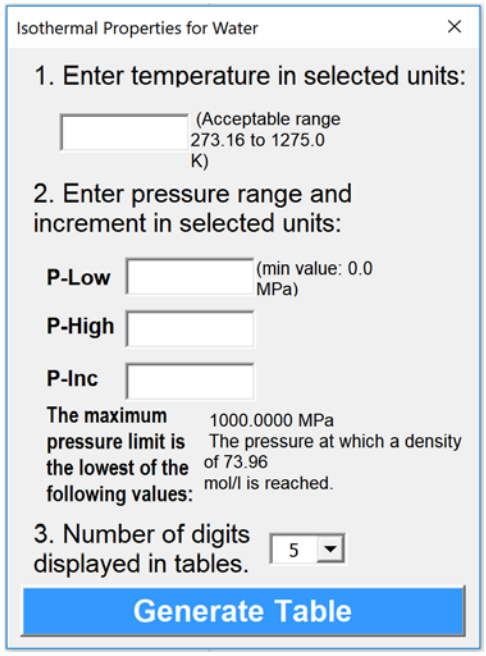

Figure 34. NIST Caddie Isothermal Data Type User Form.

The NIST Caddie add-in has some user error safeguards built in, although, the add-in is not fully coded to prevent errors. For example, the input options shown in Figure 34 will not allow the user to enter anything but numbers or a decimal after the number zero. The add-in will not prevent a user from entering values beyond the shown ranges. If a user entered a range outside the values shown, the program will crash. The author has not completed testing VBA code to prevent this error from occurring. One final feature included in this add-in is the ability for the user to view the data downloaded from the NIST webpage. Once the user has downloaded a data table, the right of the table includes links to the NIST webpages where the program downloaded the data. This allows the user the ability to validate the program downloaded the correct data.

In summary, the NIST Caddie is a useful tool that downloads and compiles thermophysical fluid properties from the NIST Chemistry Fluid WebBook into a single Excel worksheet. This tool provides researchers and educators a valid and usable data tables on any fluid provided by the National Institute of Standards and Technology.

THIS PAGE INTENTIONALLY LEFT BLANK

VI. CONCLUSION AND FUTURE WORK

This thesis presented the motivation and background for liquid air energy storage systems, description and dynamics of the current NPS LAES system, and multiple tools for use during the system conceptualization and development stage of designing a LAES system. The development of a unique system such as LAES requires systems engineers to have a basic understanding of the physics and thermodynamics of the system. The fundamental analyses conducted in this thesis provides this understanding assuming the systems engineer has some background in thermodynamics. A systems engineer can use the two papers and Excel add-in presented in this thesis in the early stages of development of a LAES system. Systems engineers conducting future modeling and simulation of a LAES system may reference the equations and methodology presented in this thesis to validate that their models are within the expected performance parameters shown.

The current LAES system in possession of NPS did not previously create liquid air as the system design intended. Previous data of test runs of this system were not available at the time of this thesis. Through the energy and exergy analysis performed in Chapter IV, the heat exchangers are a vital component of the system. It is the opinion of the author that a likely failure point in the current LAES system was the low effectiveness of the existing heat exchangers.

The Chapter III presented a closed-form solution to analyze a vast array of non-reacting binary mixtures in a modified Linde-Hampson system. The usefulness of this paper to a systems engineer is the ability to perform analysis and comparison of an array of different possible cryogenic mixtures at any varying composition. This enables the systems engineer to complete a holistic check of different binary mixtures alternative to air. Additionally, this paper enables the research into the best mixtures to act as the working fluid for the black box Q_{out} presented in the Chapter IV. A Linde-Hampson refrigeration cycle may act as this black box system and a systems engineer may use the Chapter III to find the best mixture to achieve the required heat removal.

The Chapter IV presented an energy and exergy analysis of a LAES system in order to identify optimum operating ranges. This paper found pressures of 20 to 50 MPa as the optimum pressure range exiting the air compressor. Additionally, this paper showed that the addition of a pre-cooling heat exchanger in the liquefaction subsystem and the addition of a heat exchanger to heat beyond ambient temperatures in the energy production subsystem overall increases the performance of the LAES system. The lowest pre-cooling temperature that increased performance was 150 K, at which continued cooling increased the work required of the liquefaction subsystem. Although, this temperature is impractical achieve, and therefore, a systems engineer should consider a suitable subsystem that can achieve temperatures of 200 to 250 K. The operating ranges and additional figures presented in the paper offer insights into potential measures of performance and effectiveness of the LAES system for use in development of system requirements. The current system incorporates recovery of waste heat from the compressor to heat and evaporate liquid air using an antifreeze system. This is a practical solution, although additional analysis is required to determine the antifreeze system effectiveness in heating liquid air beyond ambient pressure.

Chapter V presented the NIST Caddie Excel add-in tool. This tool interacts with the NIST webpage to download large data tables of thermophysical properties of various fluids. In order to conduct the additional research into different binary mixtures, a research would need to acquire the fluid data on these mixtures. The NIST Caddie is a perfect tool to quickly download these tables and perform calculations based on the methodology presented in the Chapter III. The NIST Caddie provides any needed resolution of data, which negates the need to conduct arduous linear interpolation of data for Excel calculations. Furthermore, other researchers and educators will find value of the NIST Caddie when there is a need to download fluid data tables into Excel for calculations and/or graphical presentations.

LAES systems are directly supportive of the goal to reduce the demand on fossil fuels stated by both the Marine Corps and U.S. Army. The work presented in this thesis provides the foundation to continue research into the design and development of a LAES system at the Naval Postgraduate School. Subsequent research includes modeling and

simulation of a LAES system, which provides additional research into the system dynamics. Additionally, modeling and simulation enables trade off analyses of different subsystems and components and the eventual optimization of a LAES system. Culminating future work would be the detailed design and building of a LAES system, followed by testing and continued optimization.

THIS PAGE INTENTIONALLY LEFT BLANK

APPENDIX A. NOMENCLATURE FOR CHAPTER III AND IV

1. CHAPTER III NOMENCLATURE

Nomenclature

FOM	figure of merit
h	enthalpy (kJ/kg)
$\dot{m}$	mass flow rate (kg/s)
NIST	National Institute of Standards and Technology
p	pressure (atm)
$\dot{Q}$	heat transfer rate (kW)
s	entropy (kJ/kg)
T	temperature (K)
$\dot{W}$	rate of work, or power (kW)
x	ratio of oxygen and nitrogen liquid
y	ratio of oxygen and nitrogen gas
Y	liquid yield
Z	compressibility factor

Greek

π	partial pressure (atm)

Subscripts

#	state number
c	compressor
f	liquid state
g	gaseous state
i	ideal
N_2	nitrogen
O_2	oxygen
R	heat rejected

Figure 35. Nomenclature for Chapter III.

2. CHAPTER IV NOMENCLATURE

Nomenclature

CAES	compressed air energy storage
FOM	figure of merit
h	enthalpy (kJ/kg)
HX	heat exchanger
$\dot{I}$	exergy destruction rate
JT	Joule Thomson valve
$\dot{m}$	mass flow rate (kg/s)
LAES	liquid air energy storage
NIST	National Institute of Standards and Technology
p	pressure (atm)
PHS	pumped-hydroelectric storage
$\dot{Q}$	heat transfer rate (kW)
s	entropy (kJ/kg)
T	temperature (K)
$\dot{W}$	rate of work, or power (kW)
x	ratio of oxygen and nitrogen liquid
y	ratio of oxygen and nitrogen gas
Y	liquid yield
Z	compressibility factor

Greek

ε	exergetic efficiency
η	energy efficiency
π	partial pressure (atm)
ψ	exergy flow

Subscripts

0	dead state
#	state number
a	black-box subsystem, Q_{in}
act	actual
c	compressor
e	energy production subsystem, flow out
f	liquid state
g	gaseous state
i	ideal, flow in
N_2	nitrogen
O_2	oxygen
p	pump
pcLH	pre-cooled Linde-Hampson
r	black-box subsystem, Q_{out}
sLH	simple Linde-Hampson
sys	LAES system
t	turbine

Figure 36. Nomenclature for Chapter IV.

THIS PAGE INTENTIONALLY LEFT BLANK

APPENDIX B. SUPPLEMENTAL NIST CADDIE EXCEL ADD-IN

As described in Chapter V, the supplemental file containing the NIST Caddie is an Excel add-in that downloads large amounts of data tables from the NIST Chemistry WebBook. There are six main Excel user forms developed in support of the NIST Caddie. Figure 37 displays these user forms and user input options available on each user form. **Those interested in using the supplemental NIST Caddie Excel add-in should contact the NPS Dudley Knox Library to acquire the add-in file.**

Updates will occur to the NIST Caddie after publication of this thesis. The author intends to publish a future update to the NIST Caddie along with examples of how researchers and educators may take advantage of this tool.

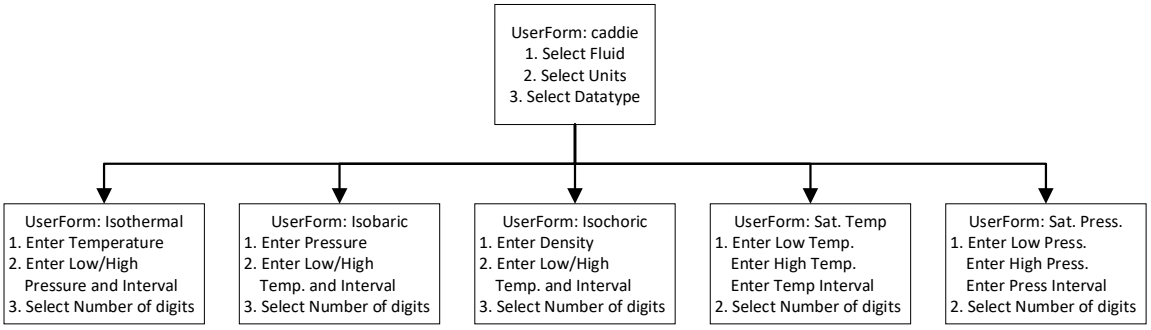

Figure 37. Six Main Excel User Forms with User Input Options in NIST Caddie

THIS PAGE INTENTIONALLY LEFT BLANK

LIST OF REFERENCES

Abdo, Rodrigo F., Hugo T.C. Pedro, Ricardo N.N. Koury, Luiz Machado, Carlos F.M. Coimbra, and Matheus P. Porto. 2015. "Performance Evaluation of Various Cryogenic Enegy Storage Systems." *Energy* 90: 1024–1032.

Airetex. 2006. "AireTex 45 High Pressure Breathing Air Compressor. Accessed October 20, 2017. http://www.airetex.com/paintball.php."

Ameel, Bernd, Christophe T'Joen, Kathleen De Kerpel, Peter De Jaeger, Henk Huisseune, Marnix Van Belleghem, and Michel De Paepe. 2013. "Thermodynamic Analysis of Energy Storage with a Liquid Air Rankine Cycle." *Applied Thermal Engineering* 52: 130–140.

ASAIE, Department of the Army. 2015. *Energy Security and Sustainability Strategy.* RefID: 2-204FF1C. March 03. https://www.army.mil/e2/c/downloads/394128.pdf.

Backhaus, Scott, Gregory W. Swift, Spyridon Chatzivasileiadis, William Tschudi, Steven Glover, Michael Starke, Jianhui Wang, Meng Yue, and Donald Hammerstrom. 2015. *DC Microgrids Scoping Study—Estimate of Technical and Economic Benefits.* LA-UR-15-22097. Los Alamos National Laboratory.

Barron, Randall F. 1985. *Cryogenic Systems.* 2nd. New York, N.Y.: Oxford University Press, Inc.

Bell, Jr J.H. 1963. *Cryogenic Engineering.* Englewood Cliffs, N.J.: Prentice-Hall Inc.

Blanchard, Benjamin S., and Wolter J. Fabrycky. 2010. *Systems Engineering and Analysis.* Upper Saddle River, N.J: Pearson.

Borri, E., A. Tafone, A. Romagnoli, and G Comodi. 2017. "A Preliminary Study on the Optimal Configuration and Operating Range of a "Microgrid Scale" Air Liquefaction Plant for Liquid Air Energy Storage." *Energy Conservation and Management* (143): 275–285. doi:10.1016/j.enconman.2017.03.079.

Buede, Dennis M. 2009. *The Engineering Design of Systems Models and Methods.* 2nd. Hoboken, N.J.: John Wiley & Sons, Inc.

Chen, Haisheng, Thang Ngoc Cong, Wei Yang, Chunqing Tan, Yongliang Li, and Yulong Ding. 2009. "Progress in Electrical Energy Storage System: A Critical Review." *Progress in Natural Science* 19: 291–312. doi:10.1016/j.pnsc.2008.07.014.

Chowdhury, S., S.P. Chowdhury, and P. Crossley. 2009. *Microgrids and Active Distribution Networks.* London: The Institution of Engineering and Technology.

Forsberg, Kevin, and Harold Mooz. 1992. "The Relationship of Systems Engineering to the Project Cycle." *Engineering Management Journal* 4 (3): 36–43. doi:10.1080/10429247.1992.11414684.

Gillespie, Louis J. 1930. "The Gibbs-Dalton Law of Partial Pressures." *Physical Review* 36: 121–131.

Giuizzi, Giuseppe Leo, Michele Manno, Ludovica Maria Tolomei, and Ruggero Maria Vitali. 2015. "Thermodynamic Analysis of a Liquid Air Energy Storage System." *Energy* 93: 1639–1647.

Gökçeer, Tonguç, Gökmen Demirkaya, and Ricardo Vasquez Padilla. 2017. "Thermoeconomic Analysis of Liquid Air Energy Storage System." *ASME 2017 11th International Conference on Energy Sustainability.* Charlotte, North Carolina: ASME Digital Collection. 1–9.

Hands, B. A., ed. 1986. *Cryogenic Engineering.* London: Academic Press Inc.

Hatziargyriou, N., H. Asano, R. Iravani, and C. Marnay. 2007. "Microgrids." *IEEE Power and Energy Magazine* 5 (4): 78–94. doi:10.1109/MPAE.2007.376583.

Joshi, D.M., and H.K. Patel. 2015. "Analysis of Cryogenic Cycle with Process Modeling Tool: Aspen HYSYS." *Journal of Instrumentation* 10: 1–7. doi:10.1088/1748-0221/10/10/T10001.

Kanoglu, Mehmet. 2002. "Exergy Analysis of Multistage Cascade Refrigeration Cycle Used for Natural Gas Liquefaction." *International Journal of Energy Research* (26): 763–774. doi:10.1002/er.814.

Kanoglu, Mehmet, Ibrahim Dincer, and Marc A. Rosen. 2008. "Performance Analysis of Gas Liquefaction Cycles." *International Journal of Energy Research* 32: 35–43. doi:10.1002/er.1333.

Kawczyk, Piotr, Lukasz Szablowski, Krysztof Badyda, Sotirios Karellas, and Emmanuel Kakaras. 2016. "Impact of Selected Parameters on Performance of the Adiabatic Liquid Air Energy Storage System." *Journal of Power Technologies* 4: 238–244.

Kim, Y.M., and D. Favrat. 2010. "Energy and Exergy Analysis of a Micro-Compressed Air Energy Storage and Air Cycle Heating and Cooling System." *Energy* 35: 213–220. doi:10.1016/j.energy.2009.09.011.

Kim, Young-Min, Jang-Hee Lee, Seok-Joon Kim, and Daniel Favrat. 2012. "Potential and Evolution of Compressed Air Energy Storage: Energy and Exergy Analyses." *Entropy* 14 (8): 1501−1521. doi:10.3390/e14081501.

Krawczyk, Piotr, Lukasz Szablowski, Sotirios Karellas, and Emmanuel Kakars. 2018. "Comparative Thermodynamic Analysis of Compressed Air and Liquid Air Energy Storage Systems." *Energy* 142: 46–54. doi:10.1016/j.energy.2017.07.078.

Lemmon, E.W., M.O. McLinden, and D.G. Friend. n.d. *NIST Chemistry WebBook, NIST Standard Reference Database Number 69.* Eds. P.J. Linstrom and W.G. Mallard, National Institute of Standards and Technology. http://webbook.nist.gov/chemistry/fluid/.

Lemmon, Eric W., Richard T Jacobsen, Steven G. Penoncello, and Daniel G. Friend. 2000. "Thermodynamic Properties of Air and Mixtures of Nitrogen, Argon, and Oxygen From 60 to 2000 K at Pressures to 2000 MPa." *Journal of Physical and Chemical Reference Data* (American Institute of Physics) 29 (3). doi:10.1063/1.1285884.

Lim, Yvonne, Mushtak Al-Atabi, and Richard A. Williams. 2016. "Liquid Air as an Energy Storage: A Review." *Journal of Engineering Science and Technology* 11 (4): 496–515.

Linde, Carl. 1903. Process of Producing Low Temperatures, The Liquefaction of Gases, and the Separation of the Constituents. United States Patent 727,650. May 12.

Lior, Noam, and Na Zhang. 2007. "Energy, Exergy, and Second Law Performance Criteria." *Energy* 32: 281–296. doi:10.1016/j.energy.2006.01.019.

Luo, Xing, Jihong Wang, Mark Dooner, and Jonathan Clarke. 2015. "Overview of Current Development in Electrical Energy Storage Technologies and the Application Potential in Power System Operation." *Applied Energy* 137: 511–536. doi:10.1016/j.apenergy.2014.09.081.

McLarnon, Frank R., and Elton J. Cairns. 1989. "Energy Storage." *Annual Review Energy* 14: 241–271.

Moran, Michael J., and Howard N. Shapiro. 2004. *Fundamentals of Engineering Thermodynamics.* 5th. Hoboken, N.J.: John Wiley & Sons Inc.

Nitro-Turbodyne, Inc. 2016. "Operations Manual Liquid Air Energy Storage System (LAESS)." Under Noble Supply Purchase Order P659307 for Naval Facilities Command Engineering and Expeditionary Warfare Center, August 12.

Paniagua, Ignacio Lopez, Javier Rodriguez Martin, Celina Gonzalez Fernandez, Angel Jimenez Alvaro, and Rafael Nieto Carlier. 2013. "A New Simple Method for Estimate Exergy Destruction in Heat Exchangers." *Entropy* (15): 474–489. doi:10.3390/e15020474.

Pollman, Anthony. 2003. "Energy Optimization A Combat Multiplier." *Marine Corps Gazette* 69–73.

Pollman, Anthony G., and Anthony J. Gannon. 2015. "Multi-Physics Energy Approach and Demonstration Facility." *ASME 2015 9th International Conference on Energy Sustainability.* San Diego, C.A.: ASME.

Radcliffe, Jonathan, and Richard A. Williams. 2013. *Liquid Air in the Energy and Transport Systems Opportunities for Industry and Innovation in the UK.* Report No. 021, The Centre for Low Carbon Futures. http://liquidair.org.uk/files/full-report.pdf.

Rosen, Marc A., and Ibrahim Dincer. 2001. "Exergy as the Confluence of Energy, Environment, and Sustainable Development." *Exergy, an International Journal* 1 (1): 3–13. doi:10.1016/S1164-0235(01)00004-8.

Smith, E.M. 1977. "Storage of Electrical Energy Using Supercritical Liquid Air." *Proceedings of the Institution of Mechanical Engineers* 191 (1): 289–298. doi:10.1243/PIME_PROC_1977_191_035_02.

USMC. 2011. *USMC Expeditionary Energy Strategy Implementation Planning Guidance.* Arlington, VA: USMC Expeditionary Energy Office.

Wang, S.X., X.D. Xue, X.L. Zhang, J. Guo, Y. Zhou, and J.J Wang. 2015. "The Application of Cryogens in Liquid Fluid Energy Storage Systems." *Physics Procedia* 67: 728−732. doi:10.1016/j.phpro.2015.06.123.

Xue, X.D., S.X. Wang, X.L. Zhang, C. Cui, L.B. Chen, Y. Zhou, and J.J. Wang. 2015. "Thermodynamic Analysis of a Novel Liquid Air Energy Storage System." *Physics Procedia* 67: 733−738.

Yu, Jianlin, Gaolei Tian, and Zong Xu. 2009. "Exergy Analysis of a Joule-Thomson Cryogenic Refrigeration Cycle with an Ejector." *Energy* 34: 1864–1869. doi:10.1016/j.energy.2009.07.034.

INITIAL DISTRIBUTION LIST

1. Defense Technical Information Center
   Ft. Belvoir, Virginia

2. Dudley Knox Library
   Naval Postgraduate School
   Monterey, California